Effects of hyperons on the dynamical deconfinement transition in cold neutron star matter

Kei Iida[1] and Katsuhiko Sato[1,2]
[1]*Department of Physics, University of Tokyo, 7-3-1 Hongo, Bunkyo, Tokyo 113-0033, Japan*
[2]*Research Center for the Early Universe, University of Tokyo, 7-3-1 Hongo, Bunkyo, Tokyo 113-0033, Japan*
(Received 1 December 1997)

The influence of the presence of hyperons in dense hadronic matter on the quantum nucleation of quark matter is examined at low temperatures relevant to neutron star cores. We calculate the equation of state and the composition of matter before and after deconfinement by using a relativistic mean-field theory and an MIT bag model, respectively; the case in which hyperons are present in the hadronic system is considered, together with the case of the system without hyperons. We find that strangeness contained in hyperons acts to reduce a density jump at deconfinement as well as a lepton fraction in the hadronic phase. As a result of these reductions, a quark matter droplet being in a virtual or real state has its effective mass lightened and its electric charge diminished into nearly zero. The Coulomb screening of leptons on the droplet charge, which has significance to the droplet growth after nucleation in the absence of hyperons, is thus shown to be of little consequence. If the effective droplet mass is small enough to become comparable to the height of the potential barrier, the effect of relativity brings about an exponential increase in the rate of droplet formation via quantum tunneling, whereas the role played by energy dissipation in decelerating the droplet formation, dominant for matter without hyperons, becomes of less importance. Independently of the presence of hyperons, the dynamical compressibility of the hadronic phase is unlikely to affect the quantum nucleation of quark matter at temperatures found in neutron star interiors. For matter with and without hyperons, we estimate the overpressure needed to form the first droplet in the star during the compression due to stellar spin-down or mass accretion from a companion star. The temperature at which a crossover from the quantum nucleation to the Arrhenius-type thermal nucleation takes place is shown to be large compared with the temperature of matter in the core. We also determine the range of the bag-model parameters such as the bag constant, the QCD fine structure constant, and the strange quark mass where quark matter is expected to occur in the star.
[S0556-2813(98)01910-4]

PACS number(s): 26.60.+c, 12.38.Mh, 64.60.Qb, 97.60.Jd

I. INTRODUCTION

A neutron star core, at densities near and just above the normal nuclear density $n_0 \approx 0.16$ fm^{-3}, consists of uniform nuclear matter being electrically neutral and roughly in β equilibrium between its components such as neutrons, protons, electrons, and muons. For still higher densities, it is possible that various forms of matter including hyperons, meson (pion or kaon) condensates, quark matter droplets, and/or quark-gluon plasmas might become energetically favorable; their presence is predicted to play an important role in determining the structure and evolution of neutron stars [1]. Basically, these forms are thought to occur via pressure-induced phase transitions, whose nature, both static and dynamical, is still uncertain in the absence of adequate information about the properties of matter in the core such as the mutual interactions between its possible constituents and the equation of state.

The possible existence of quark matter in neutron stars started to be considered about two decades ago mainly by comparing the energies of hadronic and quark matter at zero temperature [2]. Using a separate physical description of the two phases, the transition from uniform hadronic matter to uniform quark matter, which proceeds suddenly at constant pressure, was expected to occur in the density range $\sim 5-10 n_0$. The presence of uniform quark matter would enhance neutrino luminosity and neutron star cooling via quark Urca processes [3] as well as soften the equation of state effectively [4]. However, the transition in the β-equilibrated matter, which contains two conserved charges, i.e., electric charge and baryon number, should proceed through a mixed phase persisting over a finite range of pressure, as predicted by Glendenning [5] according to Gibbs' criteria for phase equilibrium. In the low pressure regime of the mixed phase, as asserted by Glendenning [5] and Heiselberg *et al.* [6], quark matter droplets form a Coulomb lattice embedded in a sea of hadrons and in a roughly uniform sea of electrons and muons. This spatial structure can arise because the presence of strange and down quarks in the negatively charged quark phase plays a role in decreasing the electron and muon Fermi energies and in increasing the proton fraction in the positively charged hadronic phase. With increasing pressure, the shape of quark matter changes from spheres to rods and then to plates, until the part of quark matter and that of hadronic matter begin to be replaced by each other. After further changes of the shape of hadronic matter from plates to rods and then to spheres, the system turns into uniform quark matter at the highest pressure. Such structure of one- to three-dimensional periodicity, which has a characteristic length ~ 10 fm, would contribute not only to quake phenomena, possibly relevant to pulsar glitches, via its elastic properties [7], but also to enhanced neutron star cooling due to opening of the quark phase space for neutrino-generating processes that are inhibited in a translationally invariant system [8]. This sequence of geometrical structure comes from the competition between the surface and Coulomb energies,

indicating that these structural transitions are of first order. The mechanism of quark-hadron phase transitions at nonzero densities, however, has not yet been established by full QCD calculations, e.g., by Monte Carlo calculations of lattice gauge theory.

Kinetics of the quark-hadron phase transitions has been studied primarily in the context of the early universe and ultrarelativistic collisions of heavy ions [9]. The astrophysical situation in which such kinetics could be significant is compression of dense stellar matter during collapse of a massive star's core, spin-down of a neutron star, or mass accretion onto a neutron star from a companion star. The deconfinement transition in hadronic matter not containing strangeness, if proceeding via homogeneous nucleation [10], begins with appearance of a critical-size droplet of two-flavor (up and down) quark matter induced by fluctuations. Since a precritical droplet moves back and forth on a time scale for strong interactions, $\sim 10^{-23}$ s, which is many orders of magnitude smaller than that for weak interactions, flavor must be conserved during the precritical situation. As a consequence, a critical droplet of three-flavor quark matter containing strange quarks is unlikely to occur in spite of its stability over two-flavor quark matter. It is expected that a critical droplet of up and down quark matter appears either via thermal activation of the energy barrier separating the initial metastable (hadronic) phase from the stable (quark) phase in configuration space at high temperatures typical of matter created in highly energetic heavy-ion collisions and in stellar collapse, or via quantum penetration of this barrier at low temperatures appropriate to neutron star cores. We also note that during the growth of the critical droplet, weak processes producing strange quarks proceed fully in the stellar interiors in contrast to the case of heavy-ion collisions.

In our recent papers [11,12], the time required to form a two-flavor quark matter droplet in a neutron star core, originally composed of nuclear matter in β equilibrium, was calculated for pressures near the point of the static deconfinement transition by using a quantum tunneling analysis incorporating the electrostatic energy and the effects of energy dissipation. It was found that the dissipation effects, governed by collisions of low-energy excitations in the hadronic phase with the droplet surface, significantly increase the degree of overpressure needed to form a droplet in the star, and that the formed droplet develops into bulk matter due to the screening of leptons on the droplet charge. We also discovered that the nucleation is likely to proceed via quantum tunneling rather than via thermal activation at temperatures below ~ 0.1 MeV typical of neutron star matter. It is of interest to note that strangeness may be present in the hadronic phase in the form of hyperons (Λ, $\Sigma^{\pm}$, Σ^{0}, etc.) [13,14] or in the form of a kaon condensate [15]. The presence of strange quarks in hyperons or kaons, altering not only the equation of state and the composition before and after deconfinement but also the quark-hadron interfacial energy, may affect the nature of the formation and growth of a quark matter droplet.

A new physics content that we consider in this paper is the influence of the presence of hyperons on the dynamical deconfinement transition that may occur in the hadronic core of a neutron star accreting matter from a companion or rotating down. We particularly evaluate at what pressure a quark matter droplet forms via quantum tunneling in the metastable phase of hadronic matter containing hyperons (hereafter referred to as hyperonic matter). For this purpose, the thermodynamic properties of hyperonic matter such as the equation of state and the composition are estimated from a relativistic mean-field theory; we use the one with the parameters incorporating a binding energy of Λ in saturated nuclear matter [16]. By using an MIT bag model for the thermodynamic properties of quark matter, we calculate not only the pressure at which a deconfinement transition from hyperonic matter in β equilibrium takes place statically subject to flavor conservation, but also the corresponding jump of baryon density. In the overpressure regime, the time needed to form a quark matter droplet is obtained using a theory of quantum nucleation developed by Lifshitz and Kagan [17]; we build into this theory the effects of Coulomb energy, special relativity, energy dissipation [18], and dynamical [19] and static compressibility. Some of these effects are found to be crucial for the formation and growth of a quark matter droplet. We then estimate the critical overpressure required to form the first quark matter droplet in a neutron star core that consists of β-stable hyperonic matter being compressed during a time scale for the spin-down or accretion. The resulting crossover temperature from the quantum tunneling to the thermal activation regime is shown to be large compared with the typical temperatures of matter in the core. By comparing the obtained critical pressure with the central pressure of the star with maximum mass, we evaluate the range of the bag-model parameters, i.e., the bag constant, the QCD fine structure constant, and the strange quark mass, where quark matter is expected to occur via deconfinement in the star.

In Sec. II, the formalism to calculate the rate of nucleation of a stable phase in a metastable phase via quantum tunneling is discussed taking into account the effects of relativity, energy dissipation, and dynamical compressibility. In Sec. III, the static properties of the deconfinement transition are examined using a relativistic mean-field theory of hadronic matter with and without hyperons and a bag model for deconfined matter. In Sec. IV, on the basis of the static properties obtained in Sec. III and the formalism described in Sec. II, the time needed to form a quark matter droplet in the metastable phase of nuclear or hyperonic matter is calculated in the overpressure regime; the critical overpressure and the quantum-thermal crossover temperature are also estimated allowing for the stellar conditions. Conclusions are given in Sec. V. In the Appendix, the quark distributions inside a droplet are considered.

II. QUANTUM NUCLEATION THEORY

In this section we first summarize a theory of quantum nucleation of a stable phase in a low-temperature first-order phase transition as advanced by Lifshitz and Kagan [17]. We then extend this theory to a relativistic regime where the effective mass of a critical-size droplet of the stable phase is comparable to the height of a potential barrier. Effects of energy dissipation [18] and dynamical compressibility [19] in the metastable phase, ignored above, are also built into the formalism to calculate the rate of quantum nucleation of the new phase. We assume in this section that the stable and

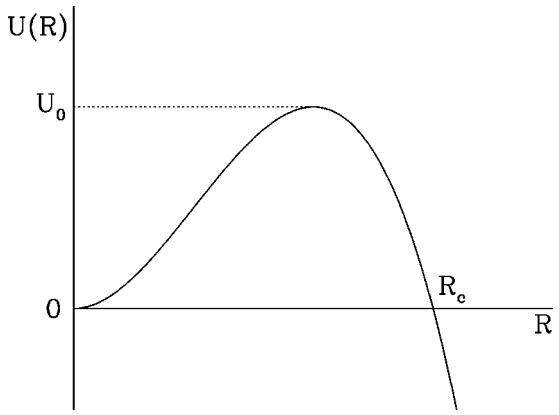

FIG. 1. Potential energy for a fluctuation of R, the radius of a spherical droplet of the stable phase in a single-component system.

metastable phases are electrically neutral quantum liquids with a single component.

A. Lifshitz-Kagan theory

Quantum tunneling nucleation of a stable phase in a first-order phase transition was first investigated by Lifshitz and Kagan [17]. Their analysis gives us a basic tool for evaluating the time needed to form a real droplet of the stable phase at low temperatures and at pressures in the vicinity of the phase equilibrium pressure. At such pressures, a nucleated droplet contains a large number of particles so that the resulting energy gain can compensate for the sharp energy increase in the interfacial layer. One may thus consider a droplet being in a virtual or real state to be a sphere macroscopically characterized by its radius $R(t)$ and describe the tunneling behavior of a virtual droplet in the semiclassical approximation. By assuming that the velocity of sound c_s is sufficiently large compared with the velocity of the phase boundary, i.e., both phases are incompressible, the potential energy for a fluctuation of the radius R may be expressed in a standard form

$$U(R)=\frac{4\pi R^3}{3}n_2(\mu_2-\mu_1)+4\pi\sigma_s R^2. \tag{1}$$

Here $\mu_1(\mu_2)$ is the chemical potential of the metastable (stable) phase calculated at fixed pressure P, n_2 is the number density of the stable phase, and σ_s is the surface tension. Expression (1) is derived from difference in the thermodynamic potential at fixed chemical potential between the initial metastable phase and the inhomogeneous phase containing a single droplet. As Fig. 1 illustrates, the potential barrier occurs between the initial metastable state and the state with a real droplet having a critical radius, $R_c=3\sigma_s/n_2(\mu_1-\mu_2)$, which satisfies $U(R_c)=0$. The height U_0 of this barrier is given by $U_0=(4/27)4\pi\sigma_s R_c^2$.

The kinetic energy for a fluctuation of R is also necessary for the determination of the quantum nucleation rate. During such a fluctuation, the density discontinuity between the stable and metastable phases induces a hydrodynamic mass flow in the medium around the droplet. The velocity field $v(r)$ is obtained from the continuity equation and the boundary condition at the droplet surface as

$$v(r)=\begin{cases}\left(1-\dfrac{n_2}{n_1}\right)\dot{R}\left(\dfrac{R}{r}\right)^2, & r\geqslant R,\\ 0, & r<R,\end{cases} \tag{2}$$

where $\dot{R}$ is the droplet growth rate, and n_1 is the number density of the metastable phase. The kinetic energy $K(R)$ is thus given by

$$K(R)=\frac{1}{2}M(R)\dot{R}^2, \tag{3}$$

where $M(R)$ is the effective droplet mass,

$$M(R)=4\pi\rho_1\left(1-\frac{n_2}{n_1}\right)^2R^3. \tag{4}$$

Here ρ_1 is the mass density of the metastable phase.

At zero temperature, the time required to form a single droplet in the metastable phase may be calculated within the WKB approximation [20] by using the Lagrangian for the fluctuating droplet

$$L(R,\dot{R})=\frac{1}{2}M(R)\dot{R}^2-U(R). \tag{5}$$

Here no energy dissipation in the medium around the droplet is considered. The energy E_0 for the zeroth bound state around $R=0$ is obtained from the Bohr quantization condition

$$I(E_0)=\frac{3}{2}\pi\hbar, \tag{6}$$

where $I(E)$ is the action for the zero-point oscillation

$$I(E)=2\int_0^{R_-}dR\sqrt{2M(R)[E-U(R)]}, \tag{7}$$

with the smaller classical turning radius R_-. The corresponding oscillation frequency ν_0 and probability of barrier penetration p_0 are given by

$$\nu_0^{-1}=\left.\frac{dI}{dE}\right|_{E=E_0} \tag{8}$$

and

$$p_0=\exp\left[-\frac{A(E_0)}{\hbar}\right], \tag{9}$$

where $A(E)$ is the action under the potential barrier

$$A(E)=2\int_{R_-}^{R_+}dR\sqrt{2M(R)[U(R)-E]}, \tag{10}$$

with the larger classical turning radius R_+. The formation time τ is finally calculated as

$$\tau=(\nu_0 p_0)^{-1}. \tag{11}$$

B. Effect of relativity

In case the potential barrier height U_0 divided by c^2 is as large as the effective mass $M(R_c)$ of a droplet of critical size, the effect of relativity on the quantum nucleation should be taken into account so that $|\dot{R}| \leqslant c$ may be satisfied. Since this situation will appear in Sec. IV, it is instructive to describe a relativistic version of the Lifshitz-Kagan theory. Let us here assume that the velocity field itself is small enough to ensure the nonrelativistic description given by Eq. (2). The Lagrangian may then be rewritten as

$$L(R,\dot{R}) = -M(R)c^2\sqrt{1-\left(\frac{\dot{R}}{c}\right)^2} + M(R)c^2 - U(R), \tag{12}$$

where $M(R)$ and $U(R)$ are given by Eqs. (4) and (1), respectively.

We proceed to obtain the time τ needed to form a droplet from the Lagrangian (12) in the semiclassical approximation. The Hamilton-Jacobi equation is derived from the Lagrangian (12) in a usual way as

$$(Mc^2)^2 = \left(\frac{\partial S}{\partial t} + U - Mc^2\right)^2 - \left(\frac{\partial S}{\partial R}\right)^2 c^2, \tag{13}$$

where $S(R,t)$ is the action associated with the Lagrangian (12). We perform the first quantization of Eq. (13) by replacing S with $\hbar/i$, and we thereby obtain a time-independent equation for the wave function $\psi(R)$ representing the state of energy E as

$$\left[-\hbar^2 c^2 \frac{d^2}{dR^2} + (U-E)(2Mc^2 + E - U)\right]\psi = 0. \tag{14}$$

Since Eq. (14) bears a resemblance to the nonrelativistic Schrödinger equation, we can derive the semiclassical solution to the tunneling problem described in terms of Eq. (14) by following a usual line of argument developed in the nonrelativistic case [21]. As a consequence, a set of equations for determining the formation time τ is obtained in the forms analogous to Eqs. (6)–(11). The energy E_0 for the zeroth bound state around $R=0$ is now determined from the Bohr quantization condition

$$I(E_0) = 2\pi\left(m_0 + \frac{3}{4}\right)\hbar. \tag{15}$$

Here $I(E)$, the action for the zero-point oscillation, is rewritten as

$$I(E) = \frac{2}{c}\int_0^{R_-} dR\sqrt{[2M(R)c^2 + E - U(R)][E - U(R)]}, \tag{16}$$

with the smaller classical turning radius R_-; m_0 is the integer defined as

$$m_0 = \left[\frac{I(E_{\min})}{2\pi\hbar} + \frac{1}{4}\right], \tag{17}$$

where $E_{\min}$ is the maximum value of $U(R) - 2M(R)c^2$, and $[\cdots]$ denotes the Gauss' notation. $E_{\min}$, being positive definite, yields the lower bound of the energy region where *positive-energy* states occur; by these we denote the states which ensure $2M(R)c^2 + E - U(R) \geqslant 0$ for arbitrary R. The zero-point oscillation frequency ν_0 is determined by substituting Eq. (16) into Eq. (8). On the other hand, the probability p_0 of barrier penetration at $E = E_0$ is given by Eq. (9) in which we now use the underbarrier action

$$A(E) = \frac{2}{c}\int_{R_-}^{R_+} dR\sqrt{[2M(R)c^2 + E - U(R)][U(R) - E]}, \tag{18}$$

with the larger classical turning radius R_+. The obtained results for ν_0 and p_0 lead to the formation time τ via Eq. (11). Equations (12)–(18) reduce to the nonrelativistic counterparts in the limit of $c \to \infty$. The higher order effect of relativity acts to raise the energy level and hence to enhance the tunneling probability, as will be clarified in Sec. IV.

C. Effect of energy dissipation

So far it was assumed that the system adjusts adiabatically to the fluctuation of R, i.e., a virtual droplet of the stable phase fluctuates in a reversible way. In a realistic situation, however, relaxation processes involved proceed at a finite rate; the density adjustment with varying R is necessarily accompanied by appearance of excitations in the metastable phase. These excitations give rise to dissipation of the total energy of the droplet until the system reaches a complete thermodynamic equilibrium. If the mean free path l of the excitations is much smaller than R, the excitations play a role in viscous transport of momentum from the high to the low velocity region with the rate of energy dissipation,

$$\frac{dE}{dt} = 4\pi\eta\left(r^2\frac{dv^2}{dr}\right)_{r=R+0} = -16\pi\eta\left(1 - \frac{n_2}{n_1}\right)^2 R\dot{R}^2, \tag{19}$$

where η is the viscosity of the metastable phase and $v(r)$ is given by Eq. (2). This energy dissipation is thus built into the equation of motion for the droplet derived from Eqs. (5) or (12) as an Ohmic friction force

$$F = -16\pi\eta\left(1 - \frac{n_2}{n_1}\right)^2 R\dot{R}. \tag{20}$$

In the case in which $l \sim R$, however, the hydrodynamic description of the dissipative processes ceases to be valid; considerations of the energy dissipation require the use of the corresponding quantum kinetic equation. In the regime $l \gg R$ where the excitations behave ballistically, they collide with the droplet surface and eventually relax in the medium far away from the droplet. The resulting momentum transfer dissipates the total energy of the droplet at a rate

$$\frac{dE}{dt} = -16\pi\alpha\eta\left(1 - \frac{n_2}{n_1}\right)^2 \frac{R^2}{l}\dot{R}^2, \tag{21}$$

where α is a factor of order unity that depends on the nature of the excitations and their interactions with the droplet surface, and thus exerts an Ohmic friction force on the droplet:

$$F=-16\pi\alpha\eta\left(1-\frac{n_2}{n_1}\right)^2\frac{R^2}{l}\dot{R}. \tag{22}$$

It is to be noted that expressions (21) and (22) are based on the hydrodynamic equation for the velocity field, which is not applicable to the situation considered here, and hence are not completely obvious.

The influence of the Ohmic dissipation described above on the quantum nucleation rate was investigated by Burmistrov and Dubovskii [18] in terms of a path-integral formalism. This formalism was pioneered by Caldeira and Leggett [22] to consider the dissipation effects on quantum tunneling in macroscopic systems; it was noted that these effects act to reduce the tunneling probability exponentially. Hereafter, we extend the estimation of the nucleation rate to the system of finite temperature T with the help of path integrals, as advanced by Larkin and Ovchinnikov [23]. The probability $p(T)$ of formation of a droplet in the medium undergoing the energy dissipation is then given by the expression similar to Eq. (9):

$$p=\exp\left[-\frac{A(T)}{\hbar}\right]. \tag{23}$$

Here $A(T)$ is the extremal value of the effective action $S_{\rm eff}$ specified in terms of an imaginary time τ':

$$\begin{aligned}S_{\rm eff}[R(\tau')]=\int_{-\hbar\beta/2}^{\hbar\beta/2}d\tau'\Bigg\{&M(R)c^2\sqrt{1+\left(\frac{\dot{R}}{c}\right)^2}-M(R)c^2\\&+U(R)+\frac{\eta}{4\pi}\int_{-\hbar\beta/2}^{\hbar\beta/2}d\tau''[\gamma(R_{\tau'})\\&-\gamma(R_{\tau''})]^2\frac{(\pi/\hbar\beta)^2}{\sin^2\pi(\tau'-\tau'')/\hbar\beta}\Bigg\},\end{aligned} \tag{24}$$

where $\beta=(k_BT)^{-1}$ is the reciprocal temperature, $R_{\tau'}$ denotes $R(\tau')$, and $\gamma(R)$, the quantity determining the nonlocal dissipation term, is evaluated from the Ohmic friction forces (20) and (22) as

$$\gamma(R)=\begin{cases}\dfrac{8\pi^{1/2}}{3}\left|1-\dfrac{n_2}{n_1}\right|R^{3/2}, & R\gg l,\\[2ex] 2(\pi\alpha)^{1/2}\left|1-\dfrac{n_2}{n_1}\right|\dfrac{R^2}{l^{1/2}}, & R\ll l.\end{cases} \tag{25}$$

The effective action (24) is accompanied by the periodic boundary condition $R(\hbar\beta/2)=R(-\hbar\beta/2)$.

Generally, one obtains two types of trajectories that extremize the effective action $S_{\rm eff}$. One of these trajectories corresponds to a τ'-independent classical trajectory $R(\tau')=2R_c/3$, along which the action amounts to $\hbar U_0/k_BT$. The nucleation described by this trajectory proceeds via thermal fluctuations. The other trajectory depends explicitly on τ' and denotes the nucleation occurring via quantum-mechanical fluctuations. This statement is evident from the fact that the corresponding extremal action $A(T)$ reduces to $A(E_0)$ given by Eq. (18) in the limit of no energy dissipation and zero temperature. According as $A(T)$ dominates over $\hbar U_0/k_BT$ or not, the nucleation of the stable phase proceeds via thermal activation or via quantum tunneling. There exists an abrupt transition from the quantum tunneling to the thermal activation regime at the temperature T_0 derived from the relation

$$A(T_0)=\frac{\hbar U_0}{k_BT_0}. \tag{26}$$

For the purposes of practical application, it is useful to summarize the results for $A(T)$ in the ballistic ($R\ll l$) and nonrelativistic regime as given in Ref. [18]. In the case of weak dissipation, the dissipative processes add a relatively small quantity $A_1(T)$ to $A(E_0)$; the analytic expressions for $A(E_0)$ and $A_1(T)$ are given at $E_0=0$ by

$$A(E_0=0)=\frac{5\sqrt{2}\pi^2}{16}\left|1-\frac{n_2}{n_1}\right|\sqrt{\sigma_s\rho_1}R_c^{7/2} \tag{27}$$

and

$$A_1(T)=4\pi\alpha\left(1-\frac{n_2}{n_1}\right)^2\frac{\eta R_c^4}{l}\left[\frac{J_2}{\pi}+O(T^2)\right], \tag{28}$$

with $J_2\approx1.49$. For temperatures up to the crossover point T_0, not only does $A(E_0=0)$ retain its form (27) but also the term of order T^2 in Eq. (28) is negligible. For normal Fermi excitations in the medium, we obtain $\eta/l\sim n_1p_F$ with the Fermi momentum $p_F=\hbar(3\pi^2n_1)^{1/3}$. Here it is instructive to note that in the case of weak dissipation, the Fermi velocity $v_F=n_1p_F/\rho_1$ is negligibly small compared with the characteristic velocity $\sqrt{2U_0/M(R_c)}$ of a virtual droplet moving under the potential barrier. In the opposite case of strong dissipation [$v_F\gg\sqrt{2U_0/M(R_c)}$ for normal Fermi excitations], the dissipation effects control the dynamics of the droplet in configuration space and thus allow one to leave out the kinetic term in the effective action (24). The corresponding expression for $A(T)$ reads

$$A(T)=4\pi\alpha\left(1-\frac{n_2}{n_1}\right)^2\frac{\eta R_c^4}{l}s(T), \tag{29}$$

where $s(T)$, the normalized underbarrier action calculated along the extremal trajectory, is ≈1.3 in the temperature range including $T\leqslant T_0$.

D. Effect of dynamical compressibility

In a system where the metastable phase is more or less compressible, a finite compressibility acts to reduce a portion of the liquid taking part in the hydrodynamic mass flow and hence the overall kinetic energy, leading to an exponential increase in the quantum nucleation rate. These effects were considered by Korshunov [19] in the nonrelativistic regime ($c\gg|\dot{R}|$) by taking account of the time dependence of the velocity field. We formally extend his theory to the relativistic regime by replacing the kinetic term in the effective action (24) with

$$S_M[R(\tau')]=\int_{-\hbar\beta/2}^{\hbar\beta/2}d\tau'\left[-1+\sqrt{1+\left(\frac{\dot R}{c}\right)^2}\right]\times\left(\frac{c}{\dot R}\right)^2\int_{R(\tau')}^{\infty}dr\,4\pi\rho_1 r^2\left[\left(\frac{\partial\varphi}{\partial r}\right)^2+\frac{1}{c_s^2}\left(\frac{\partial\varphi}{\partial\tau'}\right)^2\right],\tag{30}$$

where $\varphi(r,\tau')$ is the velocity potential assumed to be spherically symmetric. The form of S_M adopted here is available when the flow velocity $|v|$ is much smaller than c_s. The extremalization of S_M in φ results in the wave equation

$$\frac{\partial^2\varphi}{\partial\tau'^2}+\frac{c_s^2}{r^2}\frac{\partial}{\partial r}\left(r^2\frac{\partial\varphi}{\partial r}\right)=0.\tag{31}$$

Equation (31) can be solved under the boundary condition at the droplet surface based on the assumption that the stable phase is incompressible:

$$\left(\frac{n_2}{n_1}-1\right)\dot R=-\left.\frac{\partial\varphi(r,\tau')}{\partial r}\right|_{r=R(\tau')}.\tag{32}$$

It is obvious from Eq. (30) that S_M reduces to the kinetic term in Eq. (24) (hereafter defined as S_K) in the incompressible limit ($|\dot R|\ll c_s$). The difference $S_C=S_M-S_K$ has a nonlocal character similar to the dissipation term in Eq. (24), as shown in Ref. [19].

The compressibility term S_C, if the trajectory involved is taken to be the extremal one obtained at $T=0$ and $E_0=0$ in the nonrelativistic and dissipationless limit, leads to the expression [19]

$$A_C(T)=-490\left(\frac{3\pi}{4}\right)^6\left(\frac{R_c}{3}\right)^9\left(1-\frac{n_2}{n_1}\right)^4\frac{\rho_1^2}{\sigma_s c_s}\left(\frac{k_BT}{\hbar}\right)^4.\tag{33}$$

Expression (33) describes just the principal term in the expansion with respect to T/T_0 and $\sqrt{2U_0/M(R_c)}/c_s$. It is noteworthy that $A_C(T)$ is proportional to $(T/T_0)^4$ for $T\ll T_0$. This behavior, attributable to the emission of the sound wave in the course of a fluctuation of the droplet radius, persists in the case in which the condition $\sqrt{2U_0/M(R_c)}\ll c_s$ is violated, the energy dissipation takes effect, and/or the droplet surface moves relativistically, as long as the time of flight of the extremal trajectory is finite for $T=0$. Here we refrain from proving such finiteness explicitly, but this is a feature generally held by problems with a mass varying with R.

III. STATIC DECONFINEMENT TRANSITION

We now estimate at what pressure hadronic matter in β equilibrium undergoes a static deconfinement transition at zero temperature subject to flavor conservation.[1] For this purpose, we first describe the bulk properties of the β-stable, zero-temperature hadronic matter with and without hyperons within the framework of a relativistic nuclear field theory [24]. Its Lagrangian density, denoting the interactions between baryons by the exchange of $\mathcal{M}$ mesons ($\mathcal{M}=\sigma,\omega,\rho$), is given by

$$\mathcal{L}=\sum_B\bar\psi_B\Big(i\gamma_\mu\partial^\mu-m_B+g_{\sigma B}\sigma-g_{\omega B}\gamma_\mu\omega^\mu-\frac{1}{2}g_{\rho B}\gamma_\mu\boldsymbol{\tau}\cdot\boldsymbol{\rho}^\mu\Big)\psi_B+\frac{1}{2}(\partial_\mu\sigma\partial^\mu\sigma-m_\sigma^2\sigma^2)-\frac{1}{4}\omega_{\mu\nu}\omega^{\mu\nu}+\frac{1}{2}m_\omega^2\omega_\mu\omega^\mu-\frac{1}{4}\boldsymbol{\rho}_{\mu\nu}\cdot\boldsymbol{\rho}^{\mu\nu}+\frac{1}{2}m_\rho^2\boldsymbol{\rho}_\mu\cdot\boldsymbol{\rho}^\mu-\mathcal{U}(\sigma)+\sum_l\bar\psi_l(i\gamma_\mu\partial^\mu-m_l)\psi_l,\tag{34}$$

with

$$\omega_{\mu\nu}=\partial_\mu\omega_\nu-\partial_\nu\omega_\mu,$$

$$\boldsymbol{\rho}_{\mu\nu}=\partial_\mu\boldsymbol{\rho}_\nu-\partial_\nu\boldsymbol{\rho}_\mu.$$

Here $\psi_{B(l)}$ is the Dirac spinor for baryons $B=p,n,\Lambda,\Sigma^+,\Sigma^-,\Sigma^0,\Xi^-,\Xi^0$ (for leptons $l=e^-,\mu^-$), $\boldsymbol{\tau}$ is the isospin operator, $g_{\mathcal{M}B}$ is the coupling constant between B baryons and $\mathcal{M}$ mesons, and m_i is the rest mass of the particle of species i ($i=B,\mathcal{M},l$). The potential $\mathcal{U}(\sigma)$, denoting the self-interactions of the scalar field and playing a role in reproducing the empirical nuclear incompressibility, takes a specific form,

$$\mathcal{U}(\sigma)=\frac{1}{3}a_1m_n(g_{\sigma N}\sigma)^3+\frac{1}{4}a_2(g_{\sigma N}\sigma)^4,\tag{35}$$

where N represents the nucleons ($N=n,p$).

From the Lagrangian density (34) we obtain a couple of the Euler-Lagrange equations with respect to the meson and baryon fields. In the mean field approximation adopted here, the meson fields are replaced by their expectation values and are determined from the classical field equations [14]

$$m_\omega^2\omega_0=\sum_B g_{\omega B}n_B,\tag{36}$$

$$m_\rho^2\rho_{30}=\sum_B g_{\rho B}\tau_{3B}n_B,\tag{37}$$

$$m_\sigma^2\sigma=-\frac{d\mathcal{U}(\sigma)}{d\sigma}+\frac{1}{2\pi^2}\sum_B g_{\sigma B}M_B^3[t_B\sqrt{1+t_B^2}-\ln(t_B+\sqrt{1+t_B^2})],\tag{38}$$

where n_B is the number density of B baryons, $M_B=m_B-g_{\sigma B}\sigma$ is the effective mass of the baryon, τ_{3B} is the third component of isospin of the baryon, and $t_B=k_{F,B}/M_B$ with the corresponding Fermi wave number $k_{F,B}=(3\pi^2n_B)^{1/3}$. Here the meson fields are constant for any space and time since the considered system is static and uniform. This system is also isotropic, leading to $\boldsymbol{\omega}=\boldsymbol{\rho_3}=0$. We have as-

[1]Hereafter, we take units in which $\hbar=c=k_B=1$.

sumed, furthermore, that the charged components of ρ mesons as well as the pions and the kaons have vanishing expectation values, as is normally the case.

The total energy density $\varepsilon_{\rm tot}$ and pressure P for the hadronic system are then calculated from the energy-momentum tensor derived from the Lagrangian density (34) as a sum of the hadronic term and the leptonic term [14]. The resulting expression for $\varepsilon_{\rm tot}$ is

$$\varepsilon_{\rm tot}=\varepsilon_H+\varepsilon_L\,, \tag{39}$$

with

$$\varepsilon_H=\mathcal{U}(\sigma)+\frac{1}{2}m_\sigma^2\sigma^2+\frac{1}{2}m_\omega^2\omega_0^2+\frac{1}{2}m_\rho^2\rho_{30}^2+\frac{1}{8\pi^2}$$
$$\times\sum_B M_B^4[(2t_B^2+1)t_B\sqrt{1+t_B^2}-\ln(t_B+\sqrt{1+t_B^2})], \tag{40}$$

$$\varepsilon_L=\frac{1}{8\pi^2}\sum_l m_l^4[(2t_l^2+1)t_l\sqrt{1+t_l^2}-\ln(t_l+\sqrt{1+t_l^2})], \tag{41}$$

where $t_l=k_{F,l}/m_l$ with the Fermi wave number of l leptons $k_{F,l}=(3\pi^2 n_l)^{1/3}$. The pressure is obtained as

$$P=P_H+P_L\,, \tag{42}$$

with

$$P_H=-\varepsilon_H+\sum_B n_B\mu_B\,, \tag{43}$$

$$P_L=-\varepsilon_L+\sum_l n_l\mu_l\,, \tag{44}$$

where

$$\mu_B=\sqrt{k_{F,B}^2+M_B^2}+g_{\omega B}\omega_0+g_{\rho B}\tau_{3B}\rho_{30} \tag{45}$$

is the chemical potential of B baryons, and

$$\mu_l=\sqrt{k_{F,l}^2+m_l^2} \tag{46}$$

is the chemical potential of l leptons. Here electrons and muons are looked upon as ideal gases; the density region considered here is high enough for the kinetic energy to dominate over the energy induced by Coulomb interactions. The pressure P is in turn related to the total energy density $\varepsilon_{\rm tot}$, equivalent to the mass density ρ, via

$$P=n_b^2\frac{\partial}{\partial n_b}\left(\frac{\varepsilon_{\rm tot}}{n_b}\right), \tag{47}$$

where $n_b=\Sigma_B n_B$ is the total baryon density of hadronic matter.

The parameters $g_{\sigma B}$, $g_{\rho B}$, $g_{\omega B}$, a_1, and a_2 contained in Eqs. (34) and (35) have been taken from the values determined by Glendenning and Moszkowski [16]. The properties of saturated nuclear matter adopted in Ref. [16] are characterized by the binding energy per nucleon (16.3 MeV), the saturation density (0.153 fm^{-3}), the symmetry energy (32.5 MeV), the incompressibility (300 MeV), and the effective nucleon mass ($0.7m_n$). In such a way as to reproduce these properties, the nucleon-meson coupling constants and the parameters determining the strength of the σ self-interactions were chosen as $g_{\sigma N}/m_\sigma=3.434$ fm, $g_{\omega N}/m_\omega=2.674$ fm, $g_{\rho N}/m_\rho=2.100$ fm, $a_1=0.00295$, and $a_2=-0.00107$. The hyperon-meson couplings, denoted by the ratios

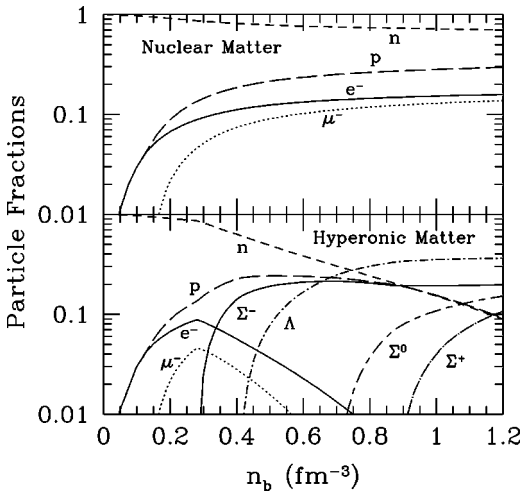

FIG. 2. Composition of β-stable nuclear matter (upper panel) and hyperonic matter (lower panel) at zero temperature, calculated using the model of Glendenning and Moszkowski [16].

$$x_{\sigma H}=\frac{g_{\sigma H}}{g_{\sigma N}},\quad x_{\omega H}=\frac{g_{\omega H}}{g_{\omega N}},\quad x_{\rho H}=\frac{g_{\rho H}}{g_{\rho N}}, \tag{48}$$

were determined mainly from the empirical Λ binding energy (28 MeV) in saturated nuclear matter as $x_{\sigma H}=x_{\rho H}=0.6$ and $x_{\omega H}=0.653$. Here the coupling constant ratios are assumed to be the same for all hyperon species. It was noted that the ratios thus chosen are compatible with the observational lower bound of the maximum neutron star mass and with the upper bound of $x_{\sigma H}$ stemming from the fit to hypernuclear levels.

In the determination of the equilibrium composition of the hadronic system at a given n_b, we need not only Eqs. (36)–(38), but also additional constraints. These are the charge neutrality condition

$$\sum_B q_B n_B-n_e-n_\mu=0, \tag{49}$$

where q_B is the electric charge of the baryon of species B, and the β-equilibrium conditions

$$\mu_B=\mu_n-q_B\mu_e\,, \tag{50}$$

$$\mu_\mu=\mu_e\,. \tag{51}$$

We have thus calculated the fraction $Y_i=n_i/n_b$ of i particles ($i=B,l$) in matter with and without hyperons; the results have been plotted as a function of n_b in Fig. 2. We can observe in this figure that the lepton fractions in hyperonic

matter are drastically reduced by the appearance of Σ^- hyperons in the density region $n_b \gtrsim 2n_0$. In Fig. 3 we have depicted the equations of state of hadronic matter as calculated allowing for and ignoring the presence of hyperons. For comparison we have also included the equations of state of equilibrium nuclear matter in the many-body calculations [25,26] based on realistic nucleon-nucleon interactions. We thus see that the presence of hyperons at high densities as predicted from the relativistic mean-field theory softens the equation of state considerably. The relativistic field theory used here automatically ensures the causality condition that the sound velocity

$$c_s = \left(\frac{\partial P}{\partial \rho}\right)^{1/2} = \left(\frac{n_b}{\rho + P}\,\frac{\partial P}{\partial n_b}\right)^{1/2} \tag{52}$$

be confined within the velocity of light.

We turn to the description of the bulk properties of uniform quark matter, deconfined from the β-stable hadronic matter mentioned above, by using an MIT bag model. We begin with the thermodynamic potential of q quarks, where $q = u$, d, and s denote up, down, and strange quarks, expressed as a sum of the kinetic term and the one-gluon-exchange term [2,27,28]

$$\begin{aligned}\Omega_q = &-\frac{1}{4\pi^2}\left[\mu_q(\mu_q^2 - m_q^2)^{1/2}\left(\mu_q^2 - \frac{5}{2}m_q^2\right)\right. \\ &\left. + \frac{3}{2}m_q^4 \ln\frac{\mu_q + (\mu_q^2 - m_q^2)^{1/2}}{m_q}\right] \\ &+ \frac{\alpha_s}{2\pi^3}\left\{3\left[\mu_q(\mu_q^2 - m_q^2)^{1/2}\right.\right. \\ &\left.\left. - m_q^2 \ln\frac{\mu_q + (\mu_q^2 - m_q^2)^{1/2}}{m_q}\right]^2 - 2(\mu_q^2 - m_q^2)^2\right\},\end{aligned} \tag{53}$$

where m_q and μ_q are the q quark rest mass and chemical potential, respectively, and α_s denotes the QCD fine structure constant. For u and d quarks, the ratios of the mass to the chemical potential are negligibly small; we thus use the following expressions in the massless limit:

$$\Omega_u = -\frac{\mu_u^4}{4\pi^2}\left(1 - \frac{2\alpha_s}{\pi}\right), \quad \Omega_d = -\frac{\mu_d^4}{4\pi^2}\left(1 - \frac{2\alpha_s}{\pi}\right). \tag{54}$$

The number density n_q of q quarks is in turn related to Ω_q via

$$n_q = -\frac{\partial \Omega_q}{\partial \mu_q}. \tag{55}$$

Then, the total energy density for the quark system is

$$\varepsilon_{\rm tot} = \varepsilon_Q + \varepsilon_L, \tag{56}$$

with

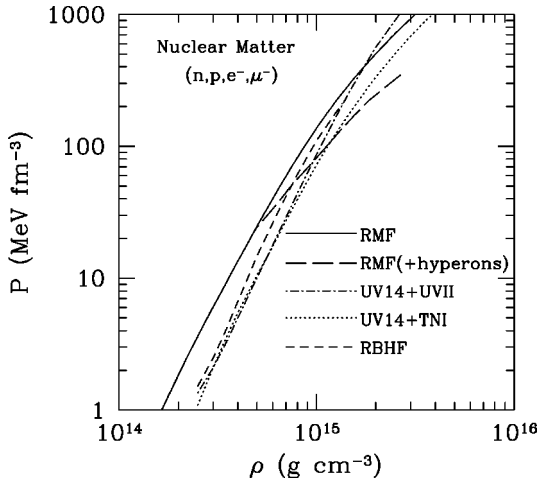

FIG. 3. Equation of state of zero-temperature nuclear matter in β equilibrium. The solid and long-dashed lines are the results calculated from the model of Glendenning and Moszkowski [16] within the relativistic mean-field (RMF) theory; the latter has been obtained allowing for the presence of hyperons. The dash-dotted and dotted lines are the results obtained by Wiringa, Fiks, and Fabrocini [25] using the Urbana v_{14} (UV14) two-nucleon potential plus the Urbana VII (UVII) three-nucleon potential and the density-dependent three-nucleon interaction (TNI) model, respectively. The short-dashed line is the relativistic Brueckner-Hartree-Fock (RBHF) result obtained by Engvik *et al.* [26] using the Bonn A two-nucleon potential.

$$\begin{aligned}\varepsilon_Q &= \sum_q (\Omega_q + \mu_q n_q) + b \\ &= \left(1 - \frac{2\alpha_s}{\pi}\right)\frac{3}{4\pi^2}(\mu_u^4 + \mu_d^4) \\ &\quad + \frac{3m_s^4}{8\pi^2}[x_s\eta_s(2x_s^2 + 1) - \ln(x_s + \eta_s)] \\ &\quad - \frac{\alpha_s m_s^4}{2\pi^3}\{2x_s^2(x_s^2 + 2\eta_s^2) - 3[x_s\eta_s + \ln(x_s + \eta_s)]^2\} + b,\end{aligned} \tag{57}$$

where $x_s = \sqrt{\mu_s^2 - m_s^2}/m_s$, $\eta_s = \sqrt{1 + x_s^2}$, ε_L is given by Eq. (41) and b is the energy density difference between the perturbative vacuum and the true vacuum, i.e., the bag constant. The total baryon density is now given by

$$n_b = \frac{1}{3}\sum_q n_q. \tag{58}$$

By using the thermodynamic relation, we obtain the pressure

$$P = P_Q + P_L, \tag{59}$$

with

$$P_Q = -\sum_q \Omega_q - b, \tag{60}$$

where P_L is given by Eq. (44).

The parameters m_s, α_s, and b are basically obtained from the fits to light-hadron spectra. However, the values of these parameters yielded by such fits do not correspond directly to the values appropriate to bulk quark matter [28]. Taking account of possible uncertainties, we set $50\ \text{MeV fm}^{-3} \leqslant b \leqslant 200\ \text{MeV fm}^{-3}$, $0 \leqslant m_s \leqslant 300$ MeV, and $0 \leqslant \alpha_s \leqslant 1$. The ranges of α_s and m_s so chosen are consistent with the results of Barnett *et al.* [29] that are inferred from experiments and renormalized at an energy scale ~ 1 GeV of interest here.

In obtaining the composition of the quark system, we take note of its relation via flavor conservation with that of the β-stable hadronic system [30]:

$$\begin{pmatrix} Y_u \\ Y_d \\ Y_s \end{pmatrix} = \begin{pmatrix} 2 & 1 & 1 & 2 & 1 & 0 & 1 & 0 \\ 1 & 2 & 1 & 0 & 1 & 2 & 0 & 1 \\ 0 & 0 & 1 & 1 & 1 & 1 & 2 & 2 \end{pmatrix} \begin{pmatrix} Y_p \\ Y_n \\ Y_\Lambda \\ Y_{\Sigma^+} \\ Y_{\Sigma^0} \\ Y_{\Sigma^-} \\ Y_{\Xi^0} \\ Y_{\Xi^-} \end{pmatrix}, \tag{61}$$

where $Y_q = n_q / n_b$ with n_b given by Eq. (58) is the fraction of q quarks in the deconfined phase. The absence of leptonic weak processes and the charge neutrality condition ensure that the fraction Y_l of l leptons remains unchanged before and after deconfinement.

Let us now proceed to obtain the pressure P_0 of the static deconfinement transition from the relation

$$\mu_b(P_0)|_{\text{hadronic phase}} = \mu_b(P_0)|_{\text{deconfined phase}}, \tag{62}$$

where

$$\mu_b = \frac{\varepsilon_{\text{tot}} + P}{n_b}, \tag{63}$$

with the corresponding total energy density ε_{tot} and total baryon density n_b is the baryon chemical potential at fixed P. We have calculated the pressures P_0 for the parametric combinations between $50\ \text{MeV fm}^{-3} \leqslant b \leqslant 200\ \text{MeV fm}^{-3}$, $m_s = 0$, 150, 300 MeV, and $0 \leqslant \alpha_s \leqslant 1$, allowing for and ignoring the presence of hyperons in the hadronic phase. Figure 4 illustrates the resultant contour plots of the pressures P_0 on the b versus α_s plane. As specific values of P_0 shown in Fig. 4, we have chosen the pressure P_{Σ^-} at which Σ^- hyperons appear in the hadronic phase, the central pressure $P_{\max}$ of the maximum-mass ($M_{\max}$) neutron star having a hadronic matter core, and the central pressure $P_{1.4}$ of the star (not including quark matter) with canonical mass $1.4 M_\odot$; these values are tabulated in Table I. P_{Σ^-} can be determined from the relation coming from Eq. (50):

$$\mu_n = \mu_{\Sigma^-}|_{n_{\Sigma^-}=0} - \mu_e, \tag{64}$$

where $\mu_{\Sigma^-}|_{n_{\Sigma^-}=0}$ denotes the energy of the lowest state for a Σ^- hyperon. The tabulated values of $P_{\max}$ and $P_{1.4}$ have been calculated from the structure of the star whose core consists of β-stable nuclear matter or hyperonic matter. In these calculations, the gravitational mass of the star observed by a distant spectator has been obtained as a function of the central pressure or mass density of the star from the general-relativistic equation of hydrostatic balance in the nonrotating configuration, i.e., the Tolman-Oppenheimer-Volkoff equation [31], and from the corresponding equation of state. The equation of state used here has been extrapolated to lower densities appropriate to matter in the crust made up of a lattice of nuclei embedded in a sea of electrons and, when present, in a sea of neutrons. Such extrapolations make only a negligible difference in determining the stellar structure,

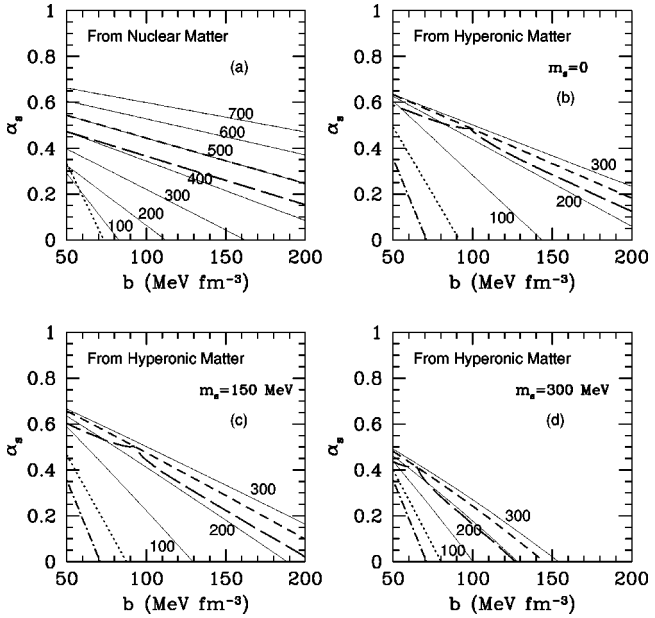

FIG. 4. Contour plots of the pressure P_0 (as marked in MeV fm^{-3}) of the static deconfinement transition on the b-α_s plane. The solid lines in (a) denote the contours of the transition pressures from β-stable nuclear matter to u and d quark matter. The solid lines in (b), (c), and (d) represent the contours of the transition pressures from β-stable hyperonic matter to u, d, and s quark matter calculated for $m_s = 0$,150,300 MeV, respectively. In each panel, the contours of $P_0 = P_{\max}$ (short-dashed line), $P_0 = P_{1.4}$ (dotted line), and $P_0 = P_{\Sigma^-}$ (dash-dotted line) are included (see text). We have also plotted the combinations of b and α_s satisfying the critical condition required to form a real quark matter droplet via deconfinement in the star that contains the nucleation centers of number $N_s = 10^{48}$ and is spinning down or accreting matter from a neighboring star in a time scale of $\tau_s = 1$ Myr. The lower b and lower α_s region is favorable for the presence of quark matter in the star. The long-dashed line in (a) denotes the result obtained for a droplet arising from nuclear matter by setting $\sigma_s = 30$ MeV fm^{-2} and $\alpha = 1$; the long-dashed line in (b)–(d), for a droplet deconfined from hyperonic matter by setting $\sigma_s = 30$ MeV fm^{-2}.

TABLE I. Values of $M_{\max}$, $P_{\max}$, $P_{1.4}$, and P_{Σ^-} evaluated for hyperonic and nuclear matter using the relativistic mean-field theory with the parameters taken from Ref. [16].

	$M_{\max}$	$P_{\max}$ (MeV fm^{-3})	$P_{1.4}$ (MeV fm^{-3})	P_{Σ^-} (MeV fm^{-3})
Hyperonic matter	$1.78 M_\odot$	261.0	43.13	23.30
Nuclear matter	$2.36 M_\odot$	500.4	38.91	

since the crust contains mass of $\sim 0.01 M_{\odot}$, confined within a few percent of the total mass [32].

The effect of a finite s quark mass acts to destabilize the quark system and hence to lower the contours of various P_0 on the b versus α_s plane, as shown in Figs. 4(b)–4(d). We have found that for $m_s \lesssim 200$ MeV, such lowering is fairly small compared with the adopted range of b and α_s. Thus, we shall generally take m_s to be zero in describing the bulk properties of quark matter. We also observe in Figs. 4(a) and 4(b) that the contours of $P_0 = P_{\max}$ and $P_0 = P_{1.4}$ reveal only a weak dependence on the presence of hyperons. This result implies that within the confines of the present models for matter, the degree of strangeness-induced stabilization of the hadronic phase compensates for that of the deconfined phase as long as $m_s \lesssim 200$ MeV.

For the parameters $\alpha_s = 0.4$, $b = 100$ MeV fm^{-3}, and $m_s = 0$, we have depicted in Fig. 5 the baryon chemical potentials and total energy densities for three electrically neutral bulk phases. The first phase consists of β-stable hadronic matter with or without hyperons. The second phase is composed of the matter deconfined therefrom according to Eq. (61). Lastly, for comparison, we consider a phase of u, d, and s quark matter in β equilibrium: $\mu_d = \mu_u + \mu_e$ and $\mu_d = \mu_s$. Hereafter, we shall refer to this β-stable quark matter as strange matter.[2] It is instructive to note that strange matter composed of massless quarks satisfies $n_u = n_d = n_s$ and $n_e = n_\mu = 0$. The upper crossing shown in Fig. 5(a) [5(b)] denotes the deconfinement pressure P_0, at which the total baryon density changes as can be seen from the Maxwell equal-area construction plotted in Fig. 5(c) [5(d)]. The density discontinuity for hyperonic matter is significantly smaller than that for nuclear matter, a feature with immediate relevance to the nucleation of the deconfined phase as will be discussed in Sec. IV. We likewise observe that the presence of hyperons in the hadronic phase suppresses the chemical potential difference between deconfined and strange matter. This is because the dominance of Λ hyperons in hyperonic matter renders the quark fraction Y_q in deconfined matter similar to that in strange matter.

We conclude this section by indicating that thermal effects on the static properties of the deconfinement transition may be safely omitted at low temperatures appropriate to neutron star cores. The zero-temperature models for hadronic and quark matter, described above, hold over an even wider range of temperature, $T < 10$ MeV. This is because the relative chemical potentials $\mu_i - \mu_i|_{n_i=0}$ of i particles ($i = l, B, q$), except for minor components with particle fraction $Y_i \lesssim 0.1$ ($i = B$) or $\lesssim 0.001$ ($i = l, q$), take on a value of $\sim 30-600$ MeV, sufficiently large compared with the temperature. This temperature range will thus be considered below.

[2]Although strange matter is not related to the deconfinement transition of interest here, it would occur once a droplet of the deconfined matter forms and grows into bulk matter in a neutron star. This is because the weak process $u + d \rightarrow u + s$ converts the bulk deconfined matter into strange matter during the growth of the droplet [1].

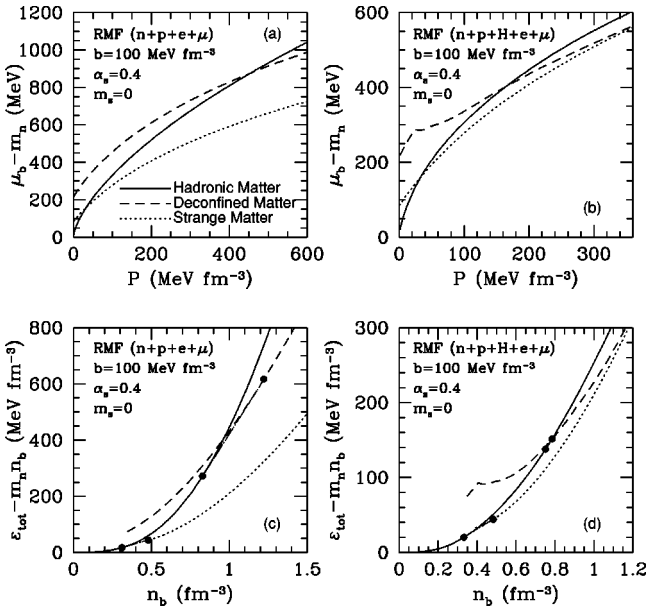

FIG. 5. (a) [(b)] Chemical potentials for the electrically neutral bulk phases as a function of pressure, calculated for the bag-model parameters $b = 100$ MeV fm^{-3}, $\alpha_s = 0.4$, and $m_s = 0$. The solid line represents the phase of β-equilibrated hadronic matter without (with) hyperons; the dashed line, the phase of matter deconfined therefrom; the dotted line, the phase of strange matter, i.e., u, d, and s quark matter in β equilibrium. (c) [(d)] Energy densities for the corresponding phases as a function of baryon density. The dash-dotted lines are the double-tangent constructions denoting the coexistence of the two bulk phases involved.

IV. DYNAMICAL DECONFINEMENT TRANSITION

In this section we first construct the effective action for the fluctuational development of a quark matter droplet in the metastable phase of hadronic matter with and without hyperons. We thereby estimate the time necessary for the quantum-mechanical formation of the first droplet in a neutron star as a function of pressure. The critical overpressure is determined in such a way as to make this formation time comparable to the time scale for the compression due to the star's spin-down or accretion; at this overpressure, the quantum-thermal crossover temperature is estimated. We finally determine the window of the bag-model parameters b, α_s, and m_s where quark matter is expected to nucleate in the star.

A. Effective action

The quantum nucleation theory described in Sec. II is directly applicable to the case in which the metastable and stable phases are electrically neutral quantum liquids with a single component. The deconfinement phase transition of interest here, however, involves matter with multiple components such as baryons, leptons, and quarks. Moreover, the inhomogeneous state of matter including a single quark matter droplet leads inevitably to a violation of the local charge neutrality, a property that is inherent in the systems (e.g., nuclei) where strong interactions compete with Coulomb interactions. It is thus necessary to generalize the quantum nucleation theory by taking into account the multiplicity of components and the electrostatic energy.

1. Nuclear matter

Let us now construct the effective action, leading to the rate of quantum nucleation of quark matter in the case in which the metastable phase consists of β-stable nuclear matter, by following a line of argument of Refs. [11,12]. We begin with the potential energy $U(R)$ which is defined in the limit of $c_s \gg |\dot{R}|$ as the minimum work needed to form a quark matter droplet of radius R in the metastable phase. Pressure equilibrium between quarks and nucleons embedded in a roughly uniform sea of leptons induces the excess positive charge inside the droplet, because the baryon density of the quark phase is larger than that of the hadronic phase by $\sim 0.1-0.7$ fm^{-3}. The charged components are in turn distributed in such a way as to screen the droplet charge. The screening efficiency of i particles ($i=e,\mu,p,u,d$) may be partially measured from their Thomas-Fermi screening length

$$\lambda_{\mathrm{TF},i}=\left(\frac{1}{4\pi q_i^2 e^2}\frac{\partial \mu_i}{\partial n_i}\right)^{1/2}, \tag{65}$$

where q_i is the electric charge of the particle of species i. For the droplet sizes of interest, $R \lesssim 10$ fm, we can assume the fluid of protons to be homogeneous since $\lambda_{\mathrm{TF},p} \gtrsim 10$ fm in the considered density range $n_b \gtrsim 4n_0$. The other components, whose screening lengths are confined within 10 fm, deviate more or less from uniformity. On the other hand, the flavor conservation, holding fixed the ratio of the number of u quarks to that of d quarks inside the droplet, makes the screening action by quarks ineffective, since u and d quarks have electric charge with opposite sign. We assume that u and d quarks are distributed uniformly; it turns out that the quark screening, i.e., the static compressibility of the fluid of quarks, does not contribute significantly to a reduction of the potential energy of the droplet (see the Appendix).

For the initial metastable phase of nuclear matter in β equilibrium under pressure P, we can obtain the total energy density $\varepsilon_{\mathrm{tot},H}$, the baryon density $n_{b,H}$, and the baryon chemical potential $\mu_{b,H}$ by using Eqs. (39), (42), and (63). We then express the energy density for the inhomogeneous phase containing a single droplet as the sum of bulk, interfacial, and Coulomb terms:

$$\begin{aligned}\varepsilon_D(r)=&\,\theta(R-r)\varepsilon_Q(n_u,n_d,n_s=0)\\&+\theta(r-R)\varepsilon_H(n_n,n_p,n_{B\neq N}=0)+\varepsilon_L[n_l(r)]\\&+\varepsilon_S(r)+\frac{1}{8\pi}\mathbf{E}(r)^2.\end{aligned} \tag{66}$$

Here r is the distance from the center of the droplet, ε_Q, ε_H, and ε_L are given by Eqs. (57), (40), and (41), respectively, $\varepsilon_S(r)$ is the increase in energy density due to the quark and nucleon distributions in the interfacial layer whose thickness we assume to be much smaller than R, and $\mathbf{E}(r)$ is the electric field. The baryon density for the inhomogeneous phase is given by

$$n_{b,D}(r)=\theta(R-r)n_{b,Q}+\theta(r-R)n_{b,H}, \tag{67}$$

where $n_{b,Q}$ is the baryon density inside the droplet determined by Eq. (58). We thus obtain the potential energy by integrating the difference in the thermodynamic potential per unit volume at chemical potential $\mu_{b,H}$ between the initial metastable phase and the inhomogeneous phase over the system volume V, which is related to P via $P=-\partial(V\varepsilon_{\mathrm{tot},H})/\partial V$, as

$$\begin{aligned}U(R)=&\int_V dV\{\varepsilon_D(r)-\varepsilon_{\mathrm{tot},H}-\mu_{b,H}[n_{b,D}(r)-n_{b,H}]\}\\=&\frac{4\pi R^3}{3}n_{b,Q}(\mu_{b,Q}-\mu_{b,H})+\Delta E_L(R)+4\pi\sigma_s R^2\\&+E_C(R),\end{aligned} \tag{68}$$

where

$$\mu_{b,Q}=\frac{\varepsilon_Q(n_u,n_d,n_s=0)+\varepsilon_L(n_{l,H})+P}{n_{b,Q}} \tag{69}$$

is the chemical potential for the quark phase and

$$\Delta E_L(R)=\int_V dV\{\varepsilon_L[n_l(r)]-\varepsilon_L(n_{l,H})\} \tag{70}$$

is the excess of the lepton energy over the initial value. Here $n_{l,H}$ is the number density of l leptons in the initial metastable phase of nuclear matter, σ_s is the surface tension, and E_C is the electrostatic energy.

Since the quark-hadron interfacial properties are poorly known at finite densities, the expression for σ_s has been taken from the Fermi-gas model for a quark matter droplet in vacuum [33] as

$$\begin{aligned}\sigma_s=\frac{3}{4\pi}\sum_q\Bigg\{&\frac{\mu_q(\mu_q^2-m_q^2)}{6}-\frac{m_q^2(\mu_q-m_q)}{3}\\&-\frac{1}{3\pi}\Bigg[\mu_q^3\tan^{-1}\frac{(\mu_q^2-m_q^2)^{1/2}}{m_q}-2\mu_q m_q(\mu_q^2-m_q^2)^{1/2}\\&+m_q^3\ln\frac{\mu_q+(\mu_q^2-m_q^2)^{1/2}}{m_q}\Bigg]\Bigg\},\end{aligned} \tag{71}$$

where α_s is set to be zero. This expression arises from the reduction in quark density of states due to the presence of the droplet surface. The typical value of σ_s for matter without strangeness is obtained as $\sigma_s \approx (3/4\pi^2)(m_u\mu_u^2+m_d\mu_d^2) \sim 10$ MeV fm^{-2}, since $m_u \sim m_d \sim 10$ MeV and $\mu_u \sim \mu_d \sim 500$ MeV. The foregoing Fermi-gas description includes neither $O(\alpha_s)$ corrections nor curvature corrections. The former have yet to be determined, while the latter destabilize a quark matter droplet in vacuum by producing an energy

$$E_{\mathrm{curv}}=\frac{R}{\pi}\sum_q \mu_q^2 \tag{72}$$

for $\mu_q \gg m_q$ and $\alpha_s = 0$ [34]. Instead of explicitly including these curvature corrections in the potential (68), we set the range of σ_s as 10 MeV fm$^{-2} \leq \sigma_s \leq 50$ MeV fm^{-2} by incorporating into σ_s the increase in the interfacial energy yielded by the curvature energy (72) of the droplet having a radius in excess of ~ 3 fm. Shell effects as encountered in nuclei are likely to appear remarkably in light quark matter droplets having a baryon number $\lesssim 10$ [28], which cannot be well described by the Fermi-gas model for finite quark matter as adopted here. Nevertheless, we may assume this model to be useful, since the baryon number contained in a virtual droplet moving under the potential barrier is $\gtrsim 10$ (typically of order 100). The contribution of nucleons to the interfacial energy, ignored here, is expected to be much smaller than that of quarks at $n_{b,H} \sim n_0$, but it is uncertain in the considered density range $n_{b,H} \sim 4-6 n_0$.

In the absence of the lepton screening on the droplet charge,

$$Z_0 e = \frac{4\pi R^3 \rho_{Q0}}{3}, \tag{73}$$

with

$$\rho_{Q0} = e\left(\frac{2n_u - n_d - n_s}{3} - n_{e,H} - n_{\mu,H} \right), \tag{74}$$

we obtain $E_C = 3Z_0^2 e^2/5R$ and

$$\Delta E_L = Z_0 \mu_{e,H}, \tag{75}$$

where $\mu_{e,H}$ is the chemical potential of electrons in the initial metastable phase of nuclear matter; typically, $\mu_{e,H} \sim 250-300$ MeV. Here Eq. (75) reflects the fact that the global charge neutrality in the system volume V is guaranteed by the lepton gas which satisfies the β-equilibrium condition (51). The excess lepton energy ΔE_L, which is proportional to R^3, is naturally absorbed into the chemical-potential difference term in the potential (68). The number densities n_u and n_d are then determined from the flavor conservation (61) and the pressure equilibrium between quark and nuclear matter

$$P_Q = P_H - \frac{\Delta E_L}{4\pi R^3}, \tag{76}$$

where P_Q and P_H are given by Eqs. (60) and (43), respectively. In Eq. (76) the surface and Coulomb pressures arising from $4\pi\sigma_s R^2$ and $E_C(R)$ have been ignored since these pressures are much smaller than the bulk pressures P_Q and P_H.[3] n_u and n_d are thus independent of R. It is instructive to note that the flavor conservation (61) and the charge neutrality (49) in the hadronic phase result in the proportionality of ρ_{Q0} to $n_{e,H} + n_{\mu,H}$ and to $n_{b,Q}/n_{b,H} - 1$:

$$\rho_{Q0} = e(n_{e,H} + n_{\mu,H})\left(\frac{n_{b,Q}}{n_{b,H}} - 1 \right), \tag{77}$$

where the ratio $n_{b,Q}/n_{b,H}$ amounts to 1.2–1.8.

We next consider the screening action by leptons on the excess droplet charge $Z_0 e$. The number density $n_l(r)$ of l leptons, whose deviation $\delta n_l(r)$ from $n_{l,H}$ is small enough to be treated as a perturbation as will be shown below, has been determined from the linear Thomas-Fermi screening theory [35]. This determination [11] leads to

$$\delta n_l(r) = \left. \frac{\partial n_l}{\partial \mu_l} \right|_{n_l = n_{l,H}} e\phi(r) \equiv \frac{\kappa_l^2}{4\pi e^2} e\phi(r), \tag{78}$$

where $\phi(r)$ is the electrostatic potential derived from the Poisson equation $\nabla^2 \phi(r) - \kappa_L^2 \phi(r) = -4\pi\rho_{Q0}\theta(R-r)$ with the reciprocal of the screening length $\kappa_L = \sqrt{\kappa_e^2 + \kappa_\mu^2}$. Its solution reads

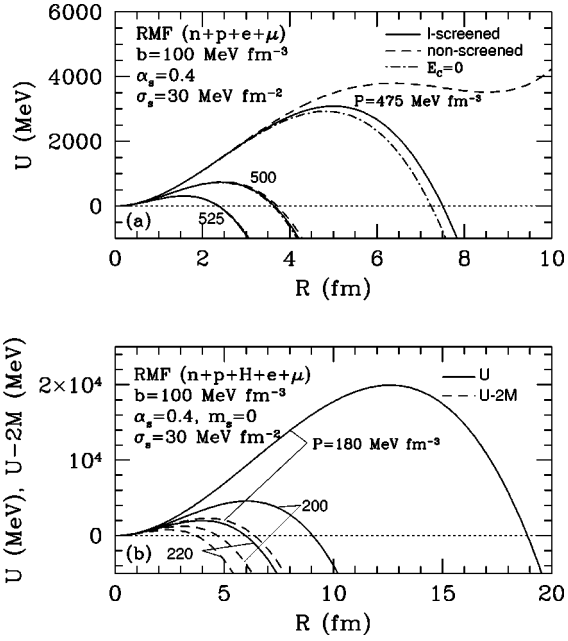

FIG. 6. Potential energies $U(R)$ of a quark matter droplet present in β-stable nuclear matter (a) and hyperonic matter (b), evaluated for the bag-model parameters $b = 100$ MeV fm^{-3}, $\alpha_s = 0.4$, and $m_s = 0$ and for various pressures above the pressure P_0 of the static deconfinement transition. In (a), we have set $\sigma_s = 30$ MeV fm^{-2}. The solid lines are the results obtained from Eq. (68) for a lepton-screened droplet; the dashed lines, for a non-screened droplet; the dash-dotted lines, in the case in which we set $E_C = 0$. The solid lines in (b) are the results evaluated from Eq. (92) for $\sigma_s = 30$ MeV fm^{-2}. The quantities $U(R) - 2M(R)$, where $M(R)$ is the effective droplet mass given by Eq. (95), have also been plotted in (b) by dashed lines. The maximum value of $U(R) - 2M(R)$ yields the upper bound of the forbidden region of the droplet energy.

[3] As long as $\sigma_s \propto n_q^{2/3}$, the surface pressure vanishes.

$$\phi(r)=\begin{cases}\dfrac{4\pi\rho_{Q0}}{\kappa_L^2}\left[1-\exp(-\kappa_L R)(1+\kappa_L R)\,\dfrac{\sinh(\kappa_L r)}{\kappa_L r}\right], & r\leqslant R,\\ \dfrac{4\pi\rho_{Q0}}{\kappa_L^2}\left[\kappa_L R\,\cosh(\kappa_L R)-\sinh(\kappa_L R)\right]\dfrac{\exp(-\kappa_L r)}{\kappa_L r}, & r>R.\end{cases} \tag{79}$$

The resulting electrostatic energy is given by

$$E_C(R)=\frac{2\pi^2\rho_{Q0}^2}{\kappa_L^5}\{-3+(\kappa_L R)^2+\exp(-2\kappa_L R)\times[3+6\kappa_L R+5(\kappa_L R)^2+2(\kappa_L R)^3]\}. \tag{80}$$

We have confirmed that the linear Thomas-Fermi approximation may be safely used; the validating condition $\mu_{e,H}\gg e\phi(r)$ is well satisfied, since $e\phi(r)/\mu_{e,H}\lesssim 0.1$ for $R\lesssim 10$ fm.[4]

Figure 6(a) exhibits the potential for the formation and growth of a quark matter droplet, characterized by $b=100$ MeV fm^{-3}, $\alpha_s=0.4$, and $\sigma_s=30$ MeV fm^{-2}, in the initial metastable phase of nuclear matter at pressures above $P_0\approx 453$ MeV fm^{-3}. This figure contains three cases in which the electrostatic energy is set to be zero, the non-screened value $3Z_0^2e^2/5R$, and the lepton-screened value given by Eq. (80). By comparing these cases, we observe that the lepton-screened case shows no dominance of the Coulomb energy over $U(R)$ for large R in contrast to the non-screened case, and agrees fairly well with the case in which $E_C=0$. This is because the cloud of leptons spreads inside the droplet and from its surface outward over a scale of the screening length $\kappa_L^{-1}\sim 5$ fm (see Fig. 9 in the Appendix). We have thus confirmed a salient feature found in Ref. [11] that the lepton screening effects prevent the formation of a Coulomb barrier which causes the droplet to remain finite. The good agreement between the lepton-screened and $E_C=0$ cases allows us to calculate the nucleation time without including E_C in the potential (68). Hereafter, we shall leave out E_C in the potential (68); the resulting potential is characterized by the critical droplet radius

$$R_c=\frac{3\sigma_s}{n_{b,Q}(\mu_{b,H}-\mu_{b,Q})-\rho_{Q0}\mu_{e,H}/e} \tag{81}$$

and by the barrier height $U_0=(4/27)4\pi\sigma_s R_c^2$.

The effective mass $M(R)$ of a quark matter droplet in β-stable nuclear matter may be estimated from the kinetic energies of nucleons and leptons, in a way analogous to that described in Sec. II A. We obtain the nucleon kinetic energy $K_H|_{n_{B\neq N}=0}$ of the form (3) by deriving the baryon velocity field from the baryon continuity equation and the boundary condition at the droplet surface; the expression for K_H is

$$K_H=2\pi\varepsilon_H(n_n,n_p,n_{B\neq N})\left(1-\frac{n_{b,Q}}{n_{b,H}}\right)^2 R^3\dot{R}^2. \tag{82}$$

By substituting the lepton distribution (78) into the lepton continuity equation, the lepton velocity field can be determined as

$$v_l(r)=-\frac{\rho_{Q0}}{n_{l,H}e}\left(\frac{\kappa_l}{\kappa_L}\right)^2\frac{\dot{R}}{(\kappa_L r)^2}\begin{cases}\kappa_L R\,\exp(-\kappa_L R)[\kappa_L r\,\cosh(\kappa_L r)-\sinh(\kappa_L r)], & r\leqslant R,\\ (\kappa_L R)^2-\kappa_L R\,\sinh(\kappa_L R)(1+\kappa_L r)\exp(-\kappa_L r), & r>R.\end{cases} \tag{83}$$

The lepton kinetic energy K_L, which is evaluated from Eq. (83) as

$$K_L<2\pi\varepsilon_L(n_{l,H})\left[\sum_l\ \frac{\kappa_l^4}{\kappa_L^4}\left(\frac{\rho_{Q0}}{n_{l,H}e}\right)^2\right]R^3\dot{R}^2, \tag{84}$$

proves negligible, partly because $\varepsilon_H(n_n,n_p,n_{B\neq N}=0)\sim 1000$ MeV fm^{-3} is much larger than $\varepsilon_L(n_{l,H})$ of order 10 MeV fm^{-3} and partly because Eq. (77) and $n_{e,H}\sim n_{\mu,H}$ ensure $(n_{b,Q}/n_{b,H}-1)^2\sim(\kappa_l^4/\kappa_L^4)(\rho_{Q0}/n_{l,H}e)^2$. The effective mass $M(R)$ is finally obtained as

$$M(R)=4\pi\varepsilon_H(n_n,n_p,n_{B\neq N}=0)\left(1-\frac{n_{b,Q}}{n_{b,H}}\right)^2 R^3. \tag{85}$$

The effect of energy dissipation discussed in Sec. II C plays a crucial role in determining the time needed to form a quark matter droplet in β-equilibrated nuclear matter, as shown in Ref. [12]. Let us now assume that the nucleons and the leptons are in a normal fluid state. Then, elementary excitations of particle species i $(i=N,l)$ appear as quasiparticles in the vicinity of their respective Fermi surfaces during a

[4]The energy increment yielded by the gradient of δn_l, present over a scale of the screening length $\kappa_L^{-1}\sim 5$ fm inward and outward from the droplet surface, is neglected in the present study.

fluctuation of R. Since the mean free path of i excitations is estimated[5] as $l_i \sim n_i^{-1/3}(\mu_i - \mu_i|_{n_i=0})^2 T^{-2} > 10^2$ fm, we can observe that each l_i is sufficiently large compared with the critical droplet radius R_c ranging typically 1–5 fm. Consequently, the nucleon and lepton excitations behave ballistically and collide with the droplet surface. The resulting transfer of momentum flux exerts on the droplet an Ohmic friction force of the form analogous to Eq. (22); this is written as a sum of nucleonic and leptonic terms

$$F = F_H|_{n_{B\neq N}=0} + F_L, \tag{86}$$

with

$$F_H = -16\pi\left(\frac{n_{b,Q}}{n_{b,H}} - 1\right)^2\left(\sum_B \alpha_B n_B k_{F,B}\right)R^2\dot{R}, \tag{87}$$

$$F_L = -16\pi f(\kappa_L R)\left[\sum_l \frac{\kappa_l^4}{\kappa_L^4}\left(\frac{\rho_{Q0}}{n_{l,H}e}\right)^2 \alpha_l n_{l,H} k_{F,l,H}\right]R^2\dot{R}. \tag{88}$$

Here $k_{F,l,H} = (3\pi^2 n_{l,H})^{1/3}$ is the Fermi momentum of l leptons in the metastable phase, α_i is a factor of order unity that depends on the properties of i excitations and on their interactions with the droplet surface, and $f(\kappa_L R)$ is a function that stems from the velocity field (83) occurring due to the lepton screening effects, behaves as $\propto(\kappa_L R)^3$ for $\kappa_L R \ll 1$, and monotonically approaches unity as $\kappa_L R$ increases.[6] Since $\Sigma_N n_N k_{F,N} \sim 250$–$450$ MeV fm^{-3} is one order of magnitude larger than $\Sigma_l n_{l,H} k_{F,l,H} \sim 30$–$70$ MeV fm^{-3}, we ignore the leptonic contribution (88) to the Ohmic friction force. The Fermi velocity $v_{F,H}|_{n_{B\neq N}=0}$ averaged over nucleon species, where $v_{F,H}$ is defined as

$$v_{F,H} = \frac{\Sigma_B n_B k_{F,B}}{\varepsilon_H(n_n, n_p, n_{B\neq N})}, \tag{89}$$

is $\sim 0.4c$, and hence $v_{F,H}|_{n_{B\neq N}=0}$ is in excess of $\sqrt{2U_0/M(R_c)} \sim 0.1$–$0.3c$. As a consequence, by recalling how to distinguish between weak and strong dissipation as described in Sec. II C, we find that except for $\alpha_N \ll 1$, the nucleation time is determined by the dissipative processes rather than by the reversible droplet motion.

[5]This estimate of l_i is based on the Landau theory of the Fermi liquids [36]. Here we have assumed that the coefficient C_i affixed to $n_i^{-1/3}(\mu_i - \mu_i|_{n_i=0})^2 T^{-2}$ is of order unity. However, C_i depends on the interaction between quasiparticles (i.e., the Landau parameters). For nucleons, such an interaction is repulsive in the high density region of interest here [37,38]; the values of C_N range ~ 0.1–1. For leptons, being relativistic and degenerate, polarization effects of the medium on the exchanged photons [27,39] induce attraction between quasiparticles; the values of C_l are roughly 10. These considerations of C_i do not change the conclusion $l_i \gg R_c$.

[6]Note that Eq. (86) reduces to Eq. (8) in Ref. [12] in the absence of muons and in the limit of $\kappa_L R \to \infty$. Thus, the contribution of the electron quasiparticles to the friction force was rather overestimated in Ref. [12].

The effects of relativity and dynamical compressibility as considered in Secs. II B and II D make only a negligible change in the estimates of the time necessary for the quantum nucleation of quark matter in the metastable phase of nuclear matter. This is because the droplet surface moves under the potential barrier at a velocity [typically $\sim\sqrt{2U_0/M(R_c)}$] fairly low compared with $c_s \sim 0.8c$ (nuclear matter) and $c_s \sim 0.6c$ (deconfined matter). These comparisons of velocity scales lead us to the effective action of a form similar to Eq. (24):

$$S_{\rm eff}[R(\tau')] = \int_{-\beta/2}^{\beta/2} d\tau' \left\{ U(R) + \alpha\left(1 - \frac{n_{b,Q}}{n_{b,H}}\right)^2\left(\sum_N n_N k_{F,N}\right) \times \int_{-\beta/2}^{\beta/2} d\tau''(R_{\tau'}^2 - R_{\tau''}^2)^2 \frac{(\pi/\beta)^2}{\sin^2\pi(\tau'-\tau'')/\beta}\right\}. \tag{90}$$

Here $U(R)$ is taken from Eq. (68) in which we set $E_C = 0$, and $\alpha_n = \alpha_p \equiv \alpha$ is assumed for simplicity. The extremal action $A(T)$ for the quantum nucleation is obtained in a form identical to Eq. (29) as

$$A(T) = 4\pi\alpha\left(1 - \frac{n_{b,Q}}{n_{b,H}}\right)^2\left(\sum_N n_N k_{F,N}\right)R_c^4 s(T), \tag{91}$$

where R_c is given by Eq. (81).

2. Hyperonic matter

Let us now construct the effective action for the development of a quark matter droplet in the initial metastable phase of β-equilibrated hadronic matter with hyperons. In this construction, we may utilize expressions (65)–(89) developed for matter without hyperons by identifying the quantities characterizing the metastable phase at a given P, i.e., $\varepsilon_{{\rm tot},H}$, $\mu_{b,H}$, $\mu_{e,H}$, $n_{b,H}$, and $n_{l,H}$, with those for matter with hyperons as well as by removing the constraints $n_{B\neq N} = 0$ and $n_s = 0$. Notice that the lepton fractions plotted in Fig. 2(b) are sufficiently small at baryon densities of interest, $n_{b,H} \sim 4$–$6n_0$, to confine the ratio $|\rho_{Q0}/n_{b,Q}e|$ of the electric charge to the baryon number inside the droplet within 10^{-2}. This behavior stems from the fact that the ratio $|\rho_{Q0}/n_{b,Q}e|$ is proportional to the sum of the lepton fractions $(n_{e,H} + n_{\mu,H})/n_{b,H}$, as can be seen from Eq. (77). When using expressions (65)–(89), therefore, we omit the quantities associated with electricity by setting $\rho_{Q0} = 0$. Correspondingly, the screening action by the charged components is neglected. Such an omission is valid for the droplet sizes of interest here, $R \lesssim 20$ fm. We have confirmed that for $R \gg 20$ fm, the Coulomb energy continues to be trivial due mainly to the screening action by leptons and due partly to that by charged baryons.

By noting Eqs. (68) and (69), the potential $U(R)$ for the formation and growth of a quark matter droplet in β-stable hyperonic matter has been written as

$$U(R) = \frac{4\pi R^3}{3} n_{b,Q}(\mu_{b,Q} - \mu_{b,H}) + 4\pi\sigma_s R^2, \tag{92}$$

with

$$\mu_{b,Q}=\frac{\varepsilon_Q(n_q)+\varepsilon_L(n_{l,H})+P}{n_{b,Q}}, \tag{93}$$

where $n_{b,Q}$, ε_Q, and ε_L are given by Eqs. (58), (57), and (41). Here σ_s, the surface tension, has been assumed to range from 10 to 50 MeV fm^{-2} by using the Fermi-gas expression (71); this range stems primarily from the uncertainty in m_s. The curvature term (72) contributes only a little to the interfacial energy of the droplet with typical $R \sim 5-15$ fm. The quark number densities n_u, n_d, and n_s have been obtained from the flavor conservation (61) and the pressure equilibrium between quarks and baryons $P_Q=P_H$, where P_Q and P_H are given by Eqs. (60) and (43), respectively; modification of such pressure equilibrium by the interfacial energy is negligibly small for typical R. In Fig. 6(b) we have depicted the potential energy (92), calculated for $b=100$ MeV fm^{-3}, $\alpha_s=0.4$, $m_s=0$, $\sigma_s=30$ MeV fm^{-2}, and various pressures above $P_0 \approx 163$ MeV fm^{-3}. The form of this potential is identical to the standard one denoted by Eq. (1); the critical droplet radius is given by

$$R_c=\frac{3\sigma_s}{n_{b,Q}(\mu_{b,H}-\mu_{b,Q})}, \tag{94}$$

from which the potential barrier height U_0 is determined as $U_0=(4/27)4\pi\sigma_s R_c^2$.

The effective mass $M(R)$ of a quark matter droplet in the metastable phase of hyperonic matter is then obtained from the baryon kinetic energy K_H given by Eq. (82) as

$$M(R)=4\pi\varepsilon_H(n_B)\left(1-\frac{n_{b,Q}}{n_{b,H}}\right)^2 R^3. \tag{95}$$

In this determination we ignore the lepton and quark kinetic energies since we have set $\rho_{Q0}=0$. Expression (95) does not include the relativistic effect on the hydrodynamic mass flow of baryons. As will be shown in the next paragraph, the baryon velocity field, given by Eq. (2) in which $n_1=n_{b,H}$ and $n_2=n_{b,Q}$, is far smaller than c, although the droplet motion itself is relativistic in many cases.

In constructing the effective action for the system having a quark matter droplet in β-equilibrated hyperonic matter, it is instructive to compare the velocities $|\dot{R}|$, c_s, and $v_{F,H}$ characterizing the droplet motion under the potential barrier. It is of great importance to note that over a wide range of the parameters σ_s, b, α_s, and m_s with relatively large α_s ($\gtrsim 0.2$) and σ_s ($\gtrsim 30$ MeV fm^{-2}), the density discontinuity $n_{b,Q}-n_{b,H}$ is small enough to make $\sqrt{2U_0/M(R_c)}$ higher than $0.3c$ for typical $R_c \sim 5-15$ fm. We should, therefore, take into account the effect of relativity on the quantum nucleation as mentioned in Sec. II B. The velocity of sound, $c_s \sim 0.5c$, of hyperonic matter cannot fully surpass the rate $|\dot{R}|$ of growth of a virtual droplet ranging typically $\sim 0.1-1c$. Thus, the effect of the dynamical compressibility of the metastable phase as discussed in Sec. II D is likely to have consequence to the quantum nucleation at temperatures near the quantum-thermal crossover point.[7] The absolute value of the baryon velocity field, which is less than $|(1-n_{b,Q}/n_{b,H})\dot{R}|$ [see Eq. (2)], is limited within $0.1c$. This leads us to use the effective mass $M(R)$ given by Eq. (95). The effect of energy dissipation is controlled by low-lying excitations of baryons induced by the fluctuation of R. These excitations, whose mean free paths are sufficiently large compared with typical R_c (except for minor components), collide with the droplet surface and exert the Ohmic friction force F_H given by Eq. (87) on the droplet. Here we have assumed the baryons to be in a normal fluid state, and we have ignored the negligible contributions of leptons and quarks to the energy dissipation. The Fermi velocity $v_{F,H}$ given by Eq. (89), averaged over baryon species, is estimated to be $\sim 0.3c$, so that $|\dot{R}|>v_{F,H}$ is satisfied in the relativistic regime. We thus confine ourselves to the dissipationless cases. We finally write the effective action as

$$\begin{aligned} S_{\rm eff}[R(\tau')] &= \int_{-\beta/2}^{\beta/2} d\tau' \left\{ \left(-1+\sqrt{1+\dot{R}^2}\right) \frac{1}{\dot{R}^2} \right. \\ &\times \int_{R(\tau')}^{\infty} dr\, 4\pi\varepsilon_H(n_B) r^2 \left[\left(\frac{\partial\varphi}{\partial r}\right)^2 + \frac{1}{c_s^2}\left(\frac{\partial\varphi}{\partial\tau'}\right)^2 \right] \\ &\left. + U(R) \right\}. \end{aligned} \tag{96}$$

Here $U(R)$ is given by Eq. (92), and $\varphi(r)$ is the velocity potential derived from the wave equation (31) and the boundary condition (32) in which $n_1=n_{b,H}$ and $n_2=n_{b,Q}$.

B. Nucleation time

Let us now proceed to evaluate the time τ needed to form a real quark matter droplet via quantum tunneling in the metastable phase of β-equilibrated hadronic matter with (without) hyperons, in the regime of overpressures and relatively low temperatures, by using the effective action (90) [(96)]. We may obtain τ within the exponential accuracy as

$$\tau=\nu_0^{-1}\exp(A), \tag{97}$$

where ν_0 is the frequency of the zero-point oscillation around $R=0$, and A is the corresponding extremal value of the effective action $S_{\rm eff}$. Here we have ignored the thermal effect on the pre-exponential factor of τ, since the frequencies of the higher order oscillations are logarithmically as large as ν_0. It may also be assumed that the energy dissipation and dynamical compressibility in hadronic matter have no influence on the pre-exponential factor, because the velocities $v_{F,H}$ and c_s take on nearly the same order of magnitude as the rate $|\dot{R}|$ of growth of a virtual droplet. The values

[7] In the present analysis, no attention is paid to the dynamical compressibility of the deconfined phase, which may affect the kinetic term included in the effective action through a change in the boundary condition at the droplet surface having the form (32).

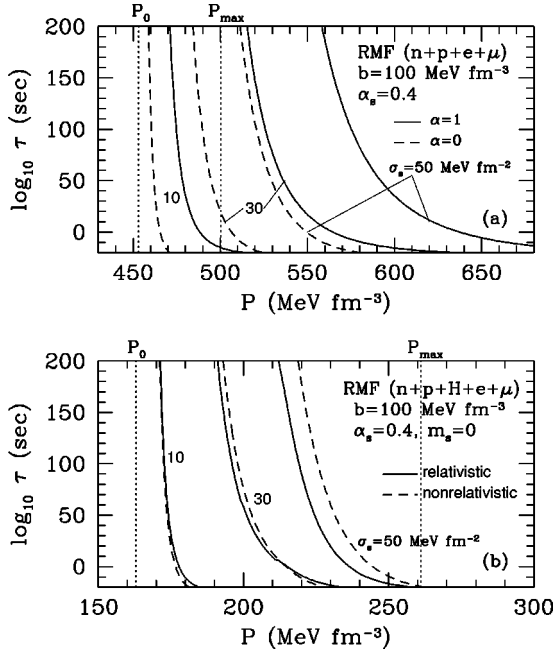

FIG. 7. Time needed to form a real quark matter droplet via quantum tunneling in β-stable zero-temperature nuclear matter (a) and hyperonic matter (b), evaluated as a function of pressure for the bag-model parameters $b=100$ MeV fm^{-3}, $\alpha_s=0.4$, and $m_s=0$. In (a), the surface tension has been set as $\sigma_s=10,30,50$ MeV fm^{-2}. The solid lines are the dissipative results obtained for $\alpha=1$, and the dashed lines are the non-dissipative results. In (b), the relativistic (solid lines) and nonrelativistic (dashed lines) results calculated for $\sigma_s=10,30,50$ MeV fm^{-2} are plotted. For comparison, we have marked in both panels the pressure P_0 of the static deconfinement transition and the central pressure $P_{\max}$ of the maximum-mass neutron star.

of ν_0^{-1} obtained by using Eq. (8) amounts to $\sim 10^{-23}$–10^{-22} s, being the time scale for strong interactions, so we set $\nu_0^{-1}=10^{-23}$ s.

In the absence of hyperons, we recall that the extremal effective action for the quantum nucleation may be roughly expressed as Eq. (91). Since the quantity $s(T)$ included in Eq. (29) depends only weakly on temperatures up to the quantum-thermal crossover value that will be found to be $\lesssim 10$ MeV, we may estimate the time τ required to form a single quark matter droplet by setting the temperature to be zero. The zero-temperature values of τ obtained for $b=100$ MeV fm^{-3}, $\alpha_s=0.4$, $m_s=0$, $\sigma_s=10,30,50$ MeV fm^{-2}, and $\alpha=1$ have been depicted in Fig. 7(a) as a function of P. With the increment in P from the pressure, $P_0\cong 453$ MeV fm^{-3}, of the static deconfinement transition, the critical droplet radius R_c decreases as Fig. 6(a) exhibits. Such behavior leads to a decrease in A ($\propto R_c^4$) and hence to an exponential reduction of τ. This indicates that at fixed P, τ decreases exponentially as $\sigma_s(\propto R_c)$ decreases linearly. As a consequence, the ambiguity in σ_s disperses the overpressure $\Delta P=P-P_0$ between ~ 30 and ~ 140 MeV fm^{-3} at a typical τ. For comparison, the formation time τ in the dissipationless case ($\alpha=0$) has also been evaluated by using the formalism written in Sec. II A; the results have been plotted in Fig. 7(a). The role of energy dissipation in increasing the overpressure ΔP needed to give a constant τ has been thus clarified.

In the case in which the hadronic phase contains hyperons, we may roughly estimate the extremal effective action by using Eq. (96). Recall that the extremal value of the compressibility term S_C is likely to behave as $\propto (T/T_0)^4$ for $T \ll T_0$, as stated in Sec. II D. Here T_0 is the quantum-thermal crossover temperature found from Eq. (26) as $A(E_0)=U_0/T_0$, where $A(E_0)$ is obtained from Eq. (18) at a given P and $T=0$. Since the value of T_0 that will be estimated to be $\gtrsim 10$ MeV is far larger than the temperature of matter in the neutron star core $T_{\rm NS}\lesssim 0.1$ MeV, we ignore the contribution of the dynamical compressibility of the hadronic phase to the extremal effective action. Thermal effects excite a droplet oscillating around $R=0$ from the ground state of energy E_0 to the mth bound state of energy E_m according to the Boltzmann distribution, and hence produce a probability of quantum-mechanical formation of a real droplet having the energy E_m, relative to the ground-state tunneling probability, as

$$p_m=\exp\left(-\frac{E_m-E_0}{T}\right)\exp[A(E_0)-A(E_m)]. \qquad (98)$$

Here $m=1,2,3,\ldots$, and E_m is determined from $I(E_m)=2\pi(m+m_0+3/4)$, where $I(E)$ and m_0 are given by Eqs. (16) and (17), respectively. At typical pressures, the difference E_m-E_{m-1} is of order 100 MeV, whereas $A(E_{m-1})-A(E_m)$ takes on a value of order 10. At $T=T_{\rm NS}$, the probability p_m is virtually zero, so we take no account of the thermal enhancement of the tunneling probability.

The nucleation time τ has been then calculated at zero temperature for hadronic matter with hyperons by substituting the potential (92) and the effective mass (95) into Eq. (18). In Fig. 7(b) we have plotted the results evaluated for $b=100$ MeV fm^{-3}, $\alpha_s=0.4$, $m_s=0$, and $\sigma_s=10,30,50$ MeV fm^{-2}, together with the nonrelativistic results obtained from Eq. (10). With increasing P from the pressure, $P_0\cong 163$ MeV fm^{-3}, of the static deconfinement transition, the potential barrier is lowered and narrowed for fixed σ_s, as illustrated in Fig. 6(b). The time τ thus shows an exponential P dependence in the overpressure regime, as Fig. 7(b) displays. We see by comparison that for large σ_s, the effect of relativity manifests itself as an exponential reduction of τ at fixed P. This feature reflects the fact that the lower bound $E_{\rm min}$ of the positive energy region, given by the maximum value of the quantity $U(R)-2M(R)$ behaving as Fig. 6(b) exhibits, renders the ratio E_0/U_0 higher than its nonrelativistic value. The larger σ_s, the more relativistically the droplet moves under the potential barrier. Accordingly, the extent of the reduction in τ develops at constant P, as can be seen from Fig. 7(b). For small σ_s, on the other hand, the nonrelativistic results for τ are slightly smaller than the relativistic results. This is because relativistic corrections act to enhance the kinetic energy of the droplet, as is evident from Eq. (12). We also observe in Fig. 7(b) that due to the uncertainty in σ_s, ΔP spreads between ~ 10 and ~ 60 MeV fm^{-3} at a typical τ.

C. Stellar conditions

We turn to the evaluation of the time needed to form the first quark matter droplet in a neutron star whose core con-

sists of β-stable hadronic matter with and without hyperons. This evaluation may be made according to τ/N_s, where N_s is the number of virtual centers of droplet formation in the star, and τ is the formation time in the hadronic system including only a single nucleation center as obtained in the preceding subsection. Here we have assumed the nucleation to be *homogeneous*: The star retains its hydrostatic equilibrium configuration during its evolution and contains no impurities leading to the formation of a seed of quark matter. N_s can be estimated as

$$N_s \sim \frac{3V_c}{4\pi R_c^3}, \tag{99}$$

where V_c is the volume of the central region in which the value of τ determined by its pressure remains within an order of magnitude of the value calculated at the star's center. The volume V_c has been obtained as $V_c \sim 10^6$ m^3, irrespective of the presence of hyperons, from the results for the pressure and density profiles of the star that were calculated in Sec. III from the Tolman-Oppenheimer-Volkoff equation and the equation of state of hadronic matter. Hereafter, we set $N_s = 10^{48}$ since R_c ranges typically $\sim 2-15$ fm. The uncertainty in N_s, expected to be an order of magnitude or so, has little consequence.

In order that the first droplet may form during a time scale for the star's spin-down or accretion $\tau_s \sim$ yr–Gyr, the overpressure should amount to such a value ΔP_c as to make τ/N_s comparable to τ_s. For example, we consider the case in which $b = 100$ MeV fm^{-3}, $\alpha_s = 0.4$, $m_s = 0$, and $\alpha = 1$ as exemplified in Fig. 7. For hadronic matter with (without) hyperons, the critical overpressure ΔP_c lies between ~ 10 (~ 30) and ~ 60 (~ 140) MeV fm^{-3} because of the uncertainty in the surface tension. Correspondingly, the critical droplet radius R_c and the potential barrier height U_0 take on a value of $\sim 9-10$ ($\sim 2.0-2.2$) fm and $\sim 2-8\times 10^3$ ($\sim 100-400$) MeV, respectively.

By using the barrier height U_0 thus evaluated, we have calculated the quantum-thermal crossover temperature T_0 from the relation $A = U_0/T_0$; the results have been plotted in Fig. 8. For comparison, we have also depicted the results obtained in the cases of strong dissipation $\alpha = 0.2$, 5 and no dissipation $\alpha = 0$ for nuclear matter as well as in the nonrelativistic case for hyperonic matter. We see from Fig. 8(a) that in the absence of hyperons, the crossover temperature T_0 is large compared with the temperature $T_{\rm NS}$ of matter in the stellar core, although the dissipation effects decrease T_0 considerably. This result suggests that the formation of a quark matter droplet in the core composed of nuclear matter, if occurring, is likely to proceed from quantum fluctuations rather than from thermal fluctuations, as is consistent with the result of Ref. [12]. Figure 8(b) shows that in the presence of hyperons, the obtained values of T_0 are again large relative to $T_{\rm NS}$, and that the effect of relativity helps to enhance T_0 for large σ_s. To be noted, however, is that the present estimate of T_0 ($\gtrsim 10$ MeV) is crude in itself. For such temperatures, the thermal effects may alter the thermodynamic quantities included in the effective action (96), induce the heat conduction by frequent collisions between the excitations, enhance the rate of quantum-mechanical formation of a droplet by raising its energy level around $R = 0$ from the ground state to the low-lying excited states, and render the dynamical compressibility of the hadronic phase effective at increasing the formation rate. At $T = T_{\rm NS}$, these effects are of little consequence, so it is safe to conclude $T_0 \gg T_{\rm NS}$. We have also confirmed that in the present calculations of T_0 allowing for and ignoring the presence of hyperons, the order of magnitude of T_0 is invariant over the adopted range of the bag-model parameters. We remark in passing that a difference in τ/N_s by 10 orders of magnitude, expected from the ambiguities in τ_s, N_s, and ν_0, alters ΔP_c, R_c, and T_0 by less than 10%.

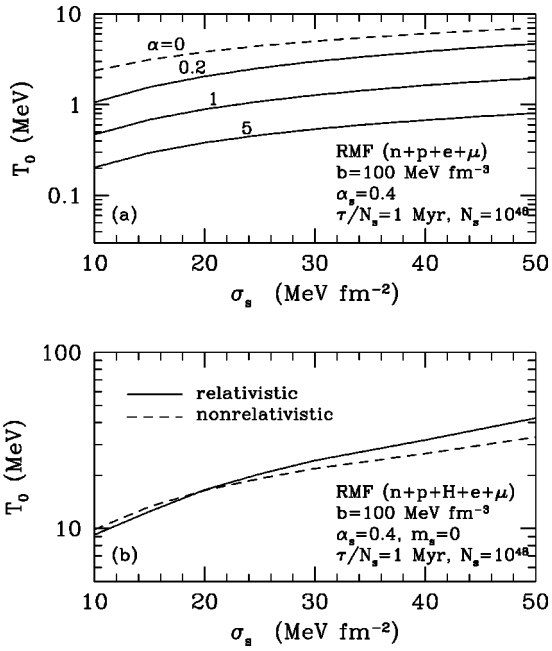

FIG. 8. Crossover temperatures T_0 from the quantum-tunneling to the thermal-activation nucleation of quark matter in β-stable nuclear matter (a) and hyperonic matter (b), calculated as a function of the surface tension for the bag-model parameters $b = 100$ MeV fm^{-3}, $\alpha_s = 0.4$, and $m_s = 0$ and for the stellar conditions $\tau/N_s = 1$ Myr and $N_s = 10^{48}$. In (a), the solid lines are the results obtained for dissipative cases of $\alpha = 0.2$, 1, 5, and the dashed line is the nondissipative result. In (b), the solid and dashed lines are the relativistic and nonrelativistic results, respectively, estimated not allowing for thermal effects on the quantum nucleation.

We finally search for the range of the bag-model parameters b, α_s, and m_s in which the quantum-tunneling nucleation of quark matter is expected to occur in the star during the compression of hadronic matter due to the stellar spin-down or accretion. Let us now consider the critical condition of the bag-model parameters for the presence of quark matter in the star: Initially, the star containing a hadronic core has a central pressure lower than $P_{\rm max}$, and subsequent compression, which increases the central pressure up to $P_{\rm max}$ in a time scale of τ_s, drives the nucleation of quark matter in the central region. Here we do not inquire whether the resulting star continues to be gravitationally stable or not. The combinations of b and α_s have been then determined for hadronic matter with and without hyperons in such a way as to satisfy the critical condition. In the absence of hyperons, we take $\alpha = 1$ and $\sigma_s = 30$ MeV fm^{-2}; in the presence of hyperons, m_s and σ_s have been set as $m_s = 0$,150,300 MeV and $\sigma_s = 30$ MeV fm^{-2}. The results have been plotted in Fig. 4. In

these four cases, the critical overpressure ΔP_c required to form the first droplet in the star results in the shrinkage of the parameter range appropriate to the presence of quark matter from that surrounded by the contour of $P_0 = P_{\max}$. We observe in the present calculations allowing for the presence of hyperons that a peak structure appears in the boundary of such a parameter range. Along this boundary, the baryon density discontinuity $n_{b,Q} - n_{b,H}$ at deconfinement runs from ~ -0.1 to ~ 0.3 fm^{-3} with changing b from 50 to 200 MeV fm^{-3}. On the way, therefore, the point at which $n_{b,Q} = n_{b,H}$ does exist. At this point, where the effective droplet mass $M(R)$ given by Eq. (95) vanishes and so does the critical overpressure ΔP_c, the boundary touches the contour of $P_0 = P_{\max}$, leading to the peak structure. It is noteworthy that around the peak where the effective mass $M(R_c)$ of the critical droplet is comparable to or smaller than the barrier height U_0, the effect of relativity on the quantum nucleation becomes prominent.

V. CONCLUSIONS

We have examined the question of how the presence of hyperons in cold dense hadronic matter affects the dynamical properties of the first-order deconfinement transition that may occur in neutron stars. For this purpose, we have used the bag-model description of quark matter and the relativistic-mean-field description of hadronic matter. The time needed to form a quark matter droplet has been then calculated by using the quantum-tunneling nucleation theory which allows for the electrostatic energy and the effects of relativity, energy dissipation, and finite compressibility.

In the calculations ignoring the presence of hyperons, we have found that the effective mass of a virtual droplet moving under the potential barrier is sufficiently large to keep its growth rate fairly small compared with the Fermi velocity averaged over nucleon species. This results in an eminent property of the quantum-tunneling formation of a real droplet: The quantum tunneling is controlled by the dissipative processes, in which the nucleon quasiparticles moving ballistically collide with the droplet surface, rather than by the reversible underbarrier motion of a droplet being in a coherent state. We have likewise found that inside a droplet of relatively small radius, an appreciable electric charge arises from the pressure equilibrium between quarks and nucleons immersed in a roughly uniform sea of electrons and muons. With increase in the droplet radius, the degenerate gas of electrons and muons becomes effective at screening the droplet charge, and at last prevents the Coulomb potential barrier from forming. This result indicates that a real droplet, if appearing, would develop into bulk matter. We note that these conclusions are consistent with the results of Refs. [11] and [12] obtained using a specific set of the bag-model parameters and a rather simplified model for nuclear matter.

The estimates allowing for the presence of hyperons have shown that the density discontinuity at deconfinement and the lepton fraction in the hadronic phase fall in magnitude considerably from the values obtained ignoring the presence of hyperons. The resulting lepton fraction is small enough for the droplet charge to be nearly zero, allowing us to assume the charge neutrality everywhere in the system. The decrease in the effective droplet mass due to the lessened density discontinuity, when sufficient, drives the droplet to move relativistically under the potential barrier. Not only does such a droplet motion cause the decelerating effect of energy dissipation on the droplet formation to decline, but also necessitates the relativistic treatment of the quantum nucleation theory. A natural extension to the relativistic regime has been made, leading to an exponential increment in the tunneling probability.

Irrespective of whether hyperons exist or not, the finite compressibility of the hadronic phase is unlikely to have consequence in decreasing the kinetic energy of a droplet via sound emission at low temperatures relevant to neutron star cores. Such temperatures have been found to be small compared with the temperature at which an abrupt transition from the quantum-tunneling to the thermal-activation nucleation takes place at a typical overpressure.

We have lastly investigated the range of the parameters b and α_s where quark matter may appear in the core of a neutron star during the compression of hadronic matter due to the stellar spin-down or accretion. It has been shown in the analysis of the static deconfinement transition that for the adopted models for bulk hadronic matter and quark matter, the existence of hyperons and the finiteness of m_s ($\lesssim 200$ MeV) do not greatly alter the favorable parameter range for the appearance of quark matter in the star. We have also found from the dynamical properties of the deconfinement transition that the critical overpressure ΔP_c required to form the first droplet in the star narrows the favorable parameter range obtained from the static properties into the lower b and lower α_s regime. The critical overpressure ΔP_c, however, is quite uncertain, because it depends on the poorly known quark-hadron interfacial properties and the unclear interactions of quasiparticles in the medium with the droplet surface. In order to make a further investigation, we should take account of the possible effect of nucleon superfluidity, which acts to decrease the number of available quasiparticle states with momenta close to the Fermi surfaces [12]. If the nucleons were in a superfluid state, the friction force exerted by the quasiparticles on the droplet and hence the critical overpressure ΔP_c in the system not containing hyperons would be reduced considerably.

It is important to bear in mind that the obtained results for the deconfinement transition are based on the adopted models for hadronic matter and for quark matter, which are inequivalent physical descriptions of the two phases and hence do not necessarily describe the transition well. Granted that such models hold good, the dynamical properties of the transition are not obvious quantitatively as mentioned in the preceding paragraph. Moreover, the mechanical or chemical impurities leading to the formation of a quark matter seed, if occurring in the star at all, might relax the condition for the transition drastically.

Once the first droplet of quark matter arises from fluctuations in a neutron star, its growth into bulk matter would cause strange matter to occupy the central region of the star as long as the strange matter is more favorable than β-equilibrated hadronic matter. These two phases, if both are present, would have a charged but overall neutral layer which spreads from the quark-hadron boundary on each side over a length scale determined by the Thomas-Fermi screening length. At the boundary, they not only would have the

same chemical potential of leptons, but also would be in equilibrium with respect to β and deconfinement processes. Even if the quark-hadron mixed phase is the lowest energy configuration at pressures around the boundary, its appearance depends on whether the boundary layer is stable against fragmentation such as the clustering of protons and of s quarks. The elucidation of this problem is beyond the scope of this paper.

We believe that the present analysis is applicable to the study of the kinetics of the deconfinement transition that may occur in hot dense matter encountered in stellar collapse and in relativistic heavy-ion collisions. Due to its high temperatures (above ~ 10 MeV), the nucleation of quark matter in hadronic matter may proceed classically, i.e., via thermal activation. Otherwise, thermally assisted quantum nucleation may take place; it may be influenced by the irreversible transport of heat and momentum in the medium and by the dynamical compressibility of the hadronic phase. In the case of stellar collapse, neutrinos trapped in a supernova core, leading to large fractions of electrons and muons, may cause a quark matter droplet to have an appreciable electric charge.

ACKNOWLEDGMENTS

This work was supported in part by Grants-in-Aid for Scientific Research provided by the Ministry of Education, Science, and Culture of Japan through Research Grant Nos. 07CE2002 and 4396.

APPENDIX: DISTRIBUTION INSIDE A QUARK MATTER DROPLET

A quark matter droplet, if having a macroscopic baryon number and a nonzero electric charge in itself, has the constituent quarks distributed over a scale of the screening length from the surface just like a conductor. In the case of a droplet of β-stable quark matter in vacuum, such a screening action by quarks was investigated by Heiselberg [40] within the linear Thomas-Fermi approximation [35]. We now extend his calculations to the case of a quark matter droplet formed in β-equilibrated nuclear matter under the flavor conservation, considered in Sec. IV A 1, and ask to what extent the resulting quark distributions alter the potential for the formation and growth of the droplet.

We begin with the potential energy $U(R)$ of a droplet of radius R given by Eq. (68), in which we remove the assumption that the quark number densities n_q $(q=u,d)$ are constant inside the droplet, and we set

$$n_q(r)=\begin{cases} n_{q0}+\delta n_q(r), & r\leqslant R, \\ 0, & r>R. \end{cases} \tag{A1}$$

Here n_{u0} and n_{d0}, independent of r, satisfy the pressure equilibrium condition (76) and the flavor conservation (61). In determining the deviations δn_q on a footing equal to δn_l, we first note that the baryon density $n_{b,D}$ and the electric charge density ρ_D for the inhomogeneous phase are written as

$$n_{b,D}(r)=\frac{1}{3}[n_u(r)+n_d(r)]+\theta(r-R)n_{b,H} \tag{A2}$$

and

$$\rho_D(r)=e\left[\sum_{i=q,l} q_i n_i(r)+\theta(r-R)n_p\right] =\theta(R-r)\rho_{Q0}+\delta\rho(r). \tag{A3}$$

Here $\delta\rho$ is the deviation of the charge density from that calculated in the incompressible limit

$$\delta\rho(r)=e\left[\theta(R-r)\sum_q q_q\delta n_q+\sum_l q_l\delta n_l\right] \tag{A4}$$

and ρ_{Q0} is given by Eq. (74) in which $n_u=n_{u0}$, $n_d=n_{d0}$, and $n_s=0$. We then expand the potential $U(R)$ up to second order in δn_q and δn_l, and minimize the resulting potential with respect to δn_q and δn_l under the global flavor conservation

$$\int_{r\leqslant R} dV(f_0\delta n_u-\delta n_d)=0, \tag{A5}$$

with $f_0=n_{d0}/n_{u0}$, and the global neutrality of electric charge

$$\sum_l \int_V dV q_l\delta n_l+\sum_q \int_{r\leqslant R} dV q_q\delta n_q+Z_0=0, \tag{A6}$$

where Z_0 is given by Eq. (73). This minimization leads not only to Eq. (78) for l leptons, but also to

$$\delta n_q=-\frac{\kappa_q^2}{4\pi(q_q e)^2}\left[q_q e\phi(r)+\mu_{q0}-\frac{1}{3}\mu_{b,H}+q_q\mu_{e,H}+C_q\right] \tag{A7}$$

for q quarks, where μ_{q0} is the chemical potential of q quarks calculated at density n_{q0},

$$\kappa_q=\left[4\pi(q_q e)^2\frac{\partial n_q}{\partial\mu_q}\bigg|_{n_q=n_{q0}}\right]^{1/2} \tag{A8}$$

is the reciprocal of the Thomas-Fermi screening length of q quarks, and $C_u=Cf_0$ and $C_d=-C$ are the constants calculated at a given R from the flavor conservation (A5). Here the proton screening continues to be ignored. We also neglect the energy increment yielded by the gradient of δn_q present over a scale of the screening length from the droplet surface. This increment, acting to flatten the quark distributions, is essentially unknown along with the quark-hadron interfacial property.

The electrostatic potential obeys the Poisson equation

$$\nabla^2\phi(r)-\kappa(r)^2\phi(r)=-4\pi\rho_Q\theta(R-r), \tag{A9}$$

where

$$\rho_Q=\rho_{Q0}-\sum_q \frac{\kappa_q^2}{4\pi q_q e}\left(\mu_{q0}-\frac{1}{3}\mu_{b,H}+q_q\mu_{e,H}+C_q\right) \tag{A10}$$

and

$$\kappa(r)=\begin{cases}\kappa_< \equiv \sqrt{\kappa_L^2+\kappa_u^2+\kappa_d^2}, & r\leqslant R,\\ \kappa_L, & r>R.\end{cases} \tag{A11}$$

Here $\kappa_<$ (κ_L) corresponds to the reciprocal of the screening length inside (outside) the droplet. The solution to Eq. (A9) is obtained as

$$\phi(r)=\begin{cases}\dfrac{4\pi\rho_Q}{\kappa_<^2}\left[1-\dfrac{\kappa_<R(1+\kappa_LR)}{\kappa_LR\,\sinh(\kappa_<R)+\kappa_<R\,\cosh(\kappa_<R)}\dfrac{\sinh(\kappa_<r)}{\kappa_<r}\right], & r\leqslant R,\\ \dfrac{4\pi\rho_Q}{\kappa_<^2}\dfrac{\kappa_LR[\kappa_<R\,\cosh(\kappa_<R)-\sinh(\kappa_<R)]}{\kappa_LR\,\sinh(\kappa_<R)+\kappa_<R\,\cosh(\kappa_<R)}\dfrac{\exp[\kappa_L(R-r)]}{\kappa_Lr}, & r>R.\end{cases} \tag{A12}$$

It is straightforward to derive the electrostatic energy E_C from Eq. (A12); the result is

$$E_C(R)=\frac{4\pi^2\rho_Q^2}{\kappa_<^5}\frac{1}{[\kappa_LR\,\sinh(\kappa_<R)+\kappa_<R\,\cosh(\kappa_<R)]^2}\left\{\left[\kappa_<R+\cosh(\kappa_<R)\sinh(\kappa_<R)-\frac{2\sinh^2(\kappa_<R)}{\kappa_<R}\right](\kappa_<R)^2(1+\kappa_LR)^2\right.$$
$$\left.+\frac{\kappa_<}{\kappa_L}[\kappa_<R\,\cosh(\kappa_<R)-\sinh(\kappa_<R)]^2\kappa_LR(\kappa_LR+2)\right\}. \tag{A13}$$

The quark distributions replace the excess lepton energy $\Delta E_L(R)$ in the potential (68) with the sum of $\Delta E_L(R)$ and the excess quark energy defined as

$$\Delta E_Q(R)=\int_{r\leqslant R}dV\{\varepsilon_Q[n_q(r)]-\varepsilon_Q(n_{q0})\}. \tag{A14}$$

The linear approximation used here yields

$$\Delta E_L(R)+\Delta E_Q(R)$$
$$=Z_0\mu_{e,H}+\sum_q\left(\mu_{q0}-\frac{1}{3}\mu_{b,H}+q_q\mu_{e,H}\right)$$
$$\times\int_{r\leqslant R}\delta n_q dV. \tag{A15}$$

By using Eqs. (78), (A4), and (A7), we have calculated the density deviations δn_q, δn_l, and $\delta\rho/e$ from the values obtained not allowing for the quark or lepton screening. We have confirmed that for $R\lesssim 10$ fm, the number density of each component remains close to its constant value obtained in the incompressible limit. The results calculated for the inhomogeneous phase characterized by $b=100$ MeV fm^{-3}, $\alpha_s=0.4$, $R=2{,}5$ fm, and $P=525$ MeV fm^{-3} have been plotted in Fig. 9, together with the charge density deviation calculated allowing for the lepton screening alone as in the main text. We see from the comparison of these charge density deviations $\delta\rho$ that the quark screening does not vary the total charge distribution ρ_D significantly even for $R=5$ fm, although $\kappa_<^{-1}\sim 3$ fm is small relative to this R and to $\kappa_L^{-1}\sim 5$ fm. This result reflects the feature that under the flavor conservation, the static compressibility of the quark fluid plays a role in chemically decreasing the sum of the excess lepton and quark energies rather than in reducing the electrostatic energy via Coulomb screening. Note that $\delta n_q>0$, leading to a reduction of the sum $\Delta E_L+\Delta E_Q$ given by Eq. (A15). The resulting decrease in the potential $U(R)$ can be observed in Fig. 10 by comparing the result obtained for a

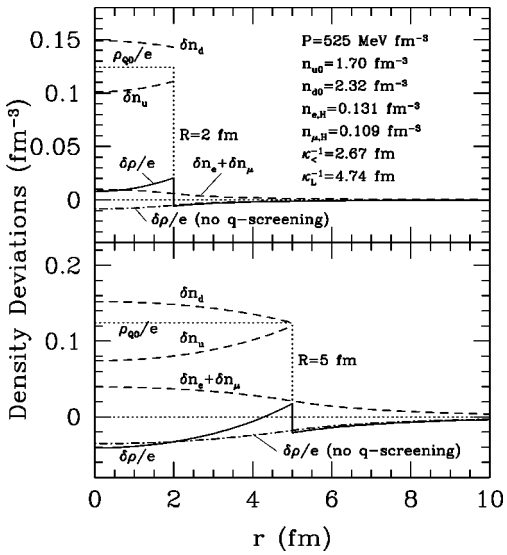

FIG. 9. Deviations δn_u, δn_d, and $\delta n_e+\delta n_\mu$ of the quark and lepton number densities from the values n_{u0}, n_{d0}, and $n_{e,H}+n_{\mu,H}$ obtained in the incompressible limit due to the screening (static compressibility) of the fluids of quarks and leptons, calculated ignoring the presence of hyperons for the droplet radius $R=2$ fm (upper panel) and $R=5$ fm (lower panel), the pressure $P=525$ MeV fm^{-3}, and the bag-model parameters $b=100$ MeV fm^{-3} and $\alpha_s=0.4$. The resulting deviation $\delta\rho$ of the electric charge density from the stepwise charge distribution obtained in the incompressible limit has also been plotted, together with the result allowing for the lepton screening alone (no quark screening). Since δn_e graphically agrees with δn_μ, only the sum $\delta n_e+\delta n_\mu$ has been shown. See the text for the definition of the screening lengths $\kappa_<^{-1}$ and κ_L^{-1}.

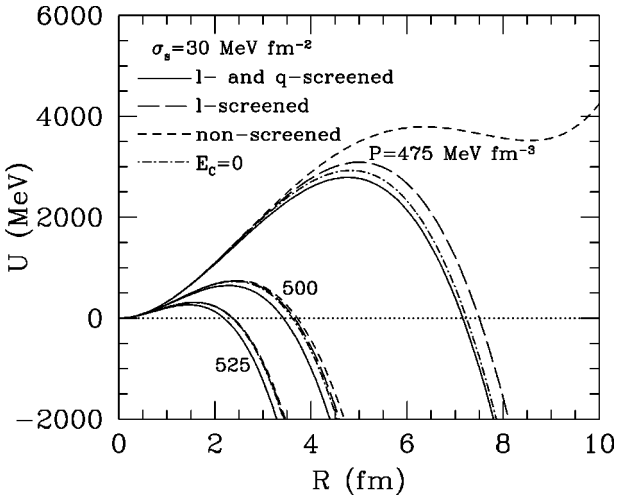

FIG. 10. Potential energies $U(R)$ of a quark matter droplet in the metastable phase of β-stable nuclear matter evaluated for the surface tension $\sigma_s=30$ MeV fm^{-2}, the bag-model parameters $b=100$ MeV fm^{-3} and $\alpha_s=0.4$, and various pressures above the pressure, $P_0\approx 453$ MeV fm^{-3}, of the static deconfinement transition. The solid lines are the results obtained from Eq. (68) for a lepton- and quark-screened droplet; the long-dashed lines, for a lepton-screened droplet; the short-dashed lines, for a nonscreened droplet; the dash-dotted lines, in the incompressible case in which we set $E_C=0$.

lepton- and quark-screened droplet with that for a lepton-screened droplet. The case of a lepton- and quark-screened droplet agrees fairly well with the case of a lepton-screened droplet and the incompressible case in which we set $E_C=0$, since the inhomogeneous phase generally satisfies

$$Z_0\mu_{e,H}\gg Z_0\mu_{e,H}-(\Delta E_L+\Delta E_Q)>E_C\gg|\Delta E_C|,$$

where E_C is given by Eq. (A13), and ΔE_C is the difference between the right-hand sides of Eqs. (80) and (A13). It is of interest to note that the finite compressibility of the fluid of N nucleons produces no chemically induced change in their number density, as can be found from the expansion of $U(R)$ up to second order in δn_N. This property is due to the β equilibrium sustained in the hadronic phase.

The shifts δn_u and δn_d due to the quark screening, being typically ~ 0.1 fm^{-3}, in turn affect the kinetic properties of the droplet. First, the effective droplet mass $M(R)$, estimated from the nucleon kinetic energy as Eq. (85), is increased, since it is proportional to the square of the baryon density discontinuity at $r=R$. Such increase in $M(R)$ diminishes the typical velocity of the precritical droplet, enforcing its smallness relative to the averaged Fermi velocity $v_{F,H}|_{n_{B\neq N}=0}$ given by Eq. (89). On the other hand, the hydrodynamic mass flow of each quark component, which arises from the Coulomb-induced inhomogeneity in δn_q, contributes little to $M(R)$. Second, the friction force $F_H|_{n_{B\neq N}=0}$ given by Eq. (87), behaving as $F_H|_{n_{B\neq N}=0}\propto M(R)$, likewise becomes strong owing to δn_q. A further friction force arises from the collisions of quark quasiparticles, carrying the quark mass flow, with the droplet surface, but this is negligibly small compared with the nucleon contribution. Recall that the baryon density discontinuity at $r=R$ is fairly large, ranging $\sim 0.1-0.7$ fm^{-3}, in the absence of the quark screening. We may then conclude that the shifts δn_q, acting to enhance the dissipation effects governed by nucleon quasiparticles, lead to a fractional increase in the critical overpressure ΔP_c.

We conclude this appendix by briefly mentioning the influence of the static compressibility of quark matter, surrounded by hadronic matter with hyperons, on the potential energy. This effect can easily be estimated by following a line of argument analogous to the case in which no hyperons exist and by neglecting the electrostatic properties. Such an estimate made over the considered range of the parameters such as b, α_s, σ_s, and m_s demonstrates that the finite compressibility increases the number densities n_u, n_d, and n_s, independently of R, by less than about 10% at typical overpressures. This leads to a chemically induced decrease in the quark energy, which has been found to be of little consequence to the potential energy. The resulting increase in the baryon density inside a droplet by typically ~ 0.05 fm^{-3} shifts the baryon kinetic energy appreciably, and hence the effective droplet mass (95). This is because, in the absence of the quark screening, the baryon density discontinuity at $r=R$ is relatively small, ranging $\sim -0.1-0.3$ fm^{-3}. Such shifts move into the lower-b regime the region of the bag-model parameters in which the droplet behaves relativistically, but otherwise do not change the qualitative conclusions about the nucleation processes obtained ignoring the quark screening.

[1] G. Baym, Nucl. Phys. **A590**, 233c (1995).
[2] J. C. Collins and M. J. Perry, Phys. Rev. Lett. **34**, 1353 (1975); G. Baym and S. A. Chin, Phys. Lett. **62B**, 241 (1976); G. Chapline and M. Nauenberg, Nature (London) **264**, 235 (1976); Phys. Rev. D **16**, 450 (1977); M. B. Kislinger and P. D. Morley, Astrophys. J. **219**, 1017 (1978); W. B. Fechner and P. C. Joss, Nature (London) **274**, 347 (1978); B. Freedman and L. McLerran, Phys. Rev. D **17**, 1109 (1978); V. Baluni, *ibid.* **17**, 2092 (1978).
[3] N. Iwamoto, Phys. Rev. Lett. **44**, 1637 (1980); Ann. Phys. (N.Y.) **141**, 1 (1982).
[4] A. Rosenhauser, E. F. Staubo, L. P. Csernai, T. Øvergård, and E. Østgaard, Nucl. Phys. **A540**, 630 (1992).
[5] N. K. Glendenning, Phys. Rev. D **46**, 1274 (1992).
[6] H. Heiselberg, C. J. Pethick, and E. F. Staubo, Phys. Rev. Lett. **70**, 1355 (1993).
[7] N. K. Glendenning and S. Pei, Phys. Rev. C **52**, 2250 (1995).
[8] M. Kiguchi and K. Sato, Prog. Theor. Phys. **66**, 725 (1981).
[9] H. Meyer-Ortmanns, Rev. Mod. Phys. **68**, 473 (1996).
[10] E. M. Lifshitz and L. P. Pitaevskii, *Physical Kinetics* (Pergamon, Oxford, 1981).
[11] K. Iida and K. Sato, Prog. Theor. Phys. **98**, 277 (1997).
[12] K. Iida, Prog. Theor. Phys. **98**, 739 (1997).
[13] H. A. Bethe and M. B. Johnson, Nucl. Phys. **A230**, 1 (1974).
[14] N. K. Glendenning, Astrophys. J. **293**, 470 (1985).
[15] D. B. Kaplan and A. E. Nelson, Phys. Lett. B **175**, 57 (1986).

[16] N. K. Glendenning and S. A. Moszkowski, Phys. Rev. Lett. **67**, 2414 (1991).
[17] I. M. Lifshitz and Yu. Kagan, Zh. Eksp. Teor. Fiz. **62**, 385 (1972) [Sov. Phys. JETP **35**, 206 (1972)].
[18] S. N. Burmistrov and L. B. Dubovskii, Zh. Eksp. Teor. Fiz. **93**, 733 (1987) [Sov. Phys. JETP **66**, 414 (1987)]; Phys. Lett. A **127**, 79 (1988).
[19] S. E. Korshunov, Fiz. Nizk. Temp. **14**, 575 (1988) [Sov. J. Low Temp. Phys. **14**, 316 (1988)].
[20] T. Nakamura and S. Takagi, Mod. Phys. Lett. B **9**, 591 (1995).
[21] E.g., A. B. Migdal and V. P. Krainov, *Approximation Methods in Quantum Mechanics* (Benjamin, New York, 1969).
[22] A. O. Caldeira and A. J. Leggett, Phys. Rev. Lett. **46**, 211 (1981).
[23] A. I. Larkin and Yu. N. Ovchinnikov, Pis'ma. Zh. Eksp. Teor. Fiz. **37**, 322 (1983) [JETP Lett. **37**, 382 (1983)]; Zh. Eksp. Teor. Fiz. **86**, 719 (1984) [Sov. Phys. JETP **59**, 420 (1984)].
[24] B. D. Serot and J. D. Walecka, Adv. Nucl. Phys. **16**, 1 (1986).
[25] R. B. Wiringa, V. Fiks, and A. Fabrocini, Phys. Rev. C **38**, 1010 (1988).
[26] L. Engvik, E. Osnes, M. Hjorth-Jensen, G. Bao, and E. Østgaard, Astrophys. J. **469**, 794 (1996).
[27] G. Baym and S. A. Chin, Nucl. Phys. **A262**, 527 (1976).
[28] E. Farhi and R. L. Jaffe, Phys. Rev. D **30**, 2379 (1984).
[29] R. M. Barnett *et al.*, Phys. Rev. D **54**, 1 (1996).
[30] M. L. Olesen and J. Madsen, Phys. Rev. D **49**, 2698 (1994).
[31] S. L. Shapiro and S. A. Teukolsky, *Black Holes, White Dwarfs, and Neutron Stars* (Wiley, New York, 1983).
[32] C. J. Pethick and D. G. Ravenhall, Annu. Rev. Nucl. Part. Sci. **45**, 429 (1995).
[33] M. S. Berger and R. L. Jaffe, Phys. Rev. C **35**, 213 (1987); **44**, 566(E) (1991).
[34] J. Madsen, Phys. Rev. Lett. **70**, 391 (1993).
[35] F. J. Dyson, Ann. Phys. (N.Y.) **63**, 1 (1971).
[36] E.g., D. Pines and P. Nozières, *The Theory of Quantum Liquids* (Benjamin, New York, 1966), Vol. I.
[37] C. J. Pethick and D. G. Ravenhall, Ann. Phys. (N.Y.) **183**, 131 (1988).
[38] R. Brockmann and R. Machleidt, Phys. Rev. C **42**, 1965 (1990).
[39] B. Jancovici, Nuovo Cimento **25**, 428 (1962).
[40] H. Heiselberg, Phys. Rev. D **48**, 1418 (1993).